water

MDPI

Article

Insight into ANN and RSM Models' Predictive Performance for Mechanistic Aspects of Cr(VI) Uptake by Layered Double Hydroxide Nanocomposites from Water

Nuhu Dalhat Mu'azu

Department of Environmental Engineering, College of Engineering, Imam Abdulrahman Bin Faisal University, Dammam 31451, Saudi Arabia; nmdalhat@iau.edu.sa or dalhat@gmail.com; Tel.: +966-507532689

Abstract: Mathematical predictive models are vital tools for understanding of pollutant uptake during adsorptive water and wastewater treatment processes. In this study, applications of CoAl-LDH and its bentonite-CoAl intercalated LDH (bentonite-CoAl-LDH) for uptake of Cr(VI) from water were modeled using response surface methodology (RSM) and artificial neural network (ANN), and their performance for predicting equilibrium, thermodynamics and kinetics of the Cr(VI) uptake were assessed and compared based on coefficient of determination (R2) and root mean square error (RMSE). The uptake of Cr(VI) fits well quartic RSM polynomial models and ANN models based on Levenberg–Marquardt algorithms (ANN-LMA). Both models predicted a better fit for the Langmuir model compared to the Freundlich model for the Cr(VI) uptake. The predicted non-linear Langmuir model contestant (K_L) values, for both the RSM and ANN-LMA models yielded better ΔG°, ΔH and ΔS predictions which supported the actual feasible, spontaneous and greater order of reaction as well as exothermic nature of Cr(VI) uptake onto the tested adsorbents. Employing the linear Langmuir model K_L values dwindles the thermodynamic parameter predictions, especially for the RSM models. The excellent kinetic parameter predictions for the ANN-LMA models further indicate a mainly pseudo-second-order process, thus confirming the predominant chemisorption mechanism as established by the Cr(VI) speciation and surface charges for the Cr(VI) uptake by both CoAl-LDH and bentonite-CoAl-LDH. The ANN-LMA models showed consistent and insignificant decline in their predictions under different mechanistic studies carried out compared to the RSM models. This study demonstrates the high potential reliability of ANN-LMA models in capturing Cr(VI) adsorption data for LDHs nanocomposite heavy metal uptake in water and wastewater treatment.

Keywords: computational intelligence; response surface methodology; adsorption modeling; adsorption equilibrium; thermodynamics; and kinetics; LDH composites; chromium aqueous adsorption; water and wastewater treatment; linear equilibrium and kinetic models; non-linear equilibrium and kinetic models

Citation: Mu'azu, N.D. Insight into ANN and RSM Models' Predictive Performance for Mechanistic Aspects of Cr(VI) Uptake by Layered Double Hydroxide Nanocomposites from Water. *Water* **2022**, *14*, 1644. https://doi.org/10.3390/w14101644

Academic Editors: Miray Bekbolet and Isabella Natali Sora

Received: 16 April 2022
Accepted: 12 May 2022
Published: 20 May 2022

1. Introduction

In the last few decades, artificial neural network (ANN) has become an indispensable modeling tool employed for understanding environmental systems as well as in a wide range of fields in various human endeavors [1–3]. This owes to the high potential predictive power of ANN compared to other mathematical techniques considering its unique generic structure and strong learning ability and retention of historical data [4,5]. This unique characteristic gives ANN unique capabilities and power for targeted response universal predictions [5]. ANN as a soft computing technique is applicable for analyzing processes through network manipulation in order to predict targeted responses of interest [4]. Additionally, implementation of ANN predictive modeling does not require specification of physico–chemical processes influencing the system. Conversely, response surface methodology (RSM) is a popular predictive modeling technique that is widely used for statistically evaluating the effects of experimental variables and their interaction

on targeted responses [6]. RSM is also employable for determination of process optimal conditions. Compared with other predictive techniques, one of the unique benefits of RSM is its requirement for a fewer number of experimental data points for implementation [6]. Moreover, RSM enables the generation of visualizable response surface models that includes curvature with capabilities of analysis of variance (ANOVA) while enabling process optimization analysis possibilities. However, the potential supremacy of ANN as a predictive modeling technique when compared to RSM has been practically demonstrated by a number of studies, and particularly for adsorption studies [7–12]. In contrast to ANN, which does not require a predetermined specified function, RSM utilizes a generalized polynomial function for model fittings [12]. Moreover, the predictability and optimization of RSM is inherently restricted within the boundary of operational conditions, rendering expansion of process understanding outside such an unfeasible boundary [2].

Globalization and increased pace of industrialization has resulted in increased production of effluent wastewater and contaminated underground water laden with heavy metals [13,14]. Heavy metals are classes of chemicals that have great potential for harming living organisms, particularly human beings due to their non-biodegradability as well as carcinogenicity and mutagenicity potentials [13]. The need for decontamination of industrial wastewater containing heavy metals below regulatory thresholds is thus a top priority for maintaining a sustainable ecosystem [15]. Even though several deployable techniques do exist, adsorption techniques have enjoyed significant acceptability and increased popularity compared with other processes for the removal of heavy metals and other forms of pollutants from wastewater. This is because adsorption processes have demonstrated unique flexibility, simplicity and applicability for different classes of pollutants with excellent performance [16,17].

Advances in nanomaterials synthesis have led to the emergence of a wide range and types of layered double hydroxide (LDH) adsorbents that are characterized by high adsorptive performances for effective water and wastewater treatment [15,16]. Represented by a general formula $[M^2{}_{1-x}\, M^3{}_x\, (OH)_2 \cdot [A^{n-}{}_{x/n} \cdot mH_2O]$ within brucite-like layers having M^2 = divalent and M^3 = trivalent metal-ions and an A^{n-} = interlayer anion, LDH are becoming favorable adsorbents for pollutant removal from aqueous phases due to their remarkable ion-exchange capabilities and recorded higher surface characteristics [18,19]. Besides, the flexibility for in-cooperating and intercalating the interlayers of LDHs layers with many materials of choice provides an unlimited window of opportunities for improving their adsorptive performance, thereby gaining further outstanding interest for researchers in water pollution control disciplines [15,19].

A number of single and composite LDH-based adsorbents synthesized using various methods have been employed for aqueous phase uptake of Cr(VI) in a number of recent studies [20–24]. In this regard, the synthesis and application of intercalated cobalt aluminum-based LDHs for removal of dye and heavy metal were reported in our earlier studies [18,25]. However, reported works on predictive modeling of adsorption onto LDHs are scarce, and the few studies that have been conducted are mainly focused on RSM techniques with a rare number of studies extended towards the application of ANN technique in predictive modeling of adsorption processes. Additionally, the majority of existing studies are more focused on dyes and organic compounds with very few dedicated to investigating heavy metal uptake onto LDHs [26]. Moreover, studies on comparative assessment of ANN and RSM performance in the few earlier reported works on adsorption studies mainly utilized limited experimental design data that are employed for RSM modeling [9].

In this study, ANN algorithms and RSM-based models were developed for predicting faced centered central composite design (FC-CCD), kinetics, equilibrium and thermodynamic adsorption data for CoAl-LDH and bentonite-CoAl intercalated layered double hydroxide (bentonite-CoAl-LDH) uptake of Cr(VI) from water. The ANN algorithm and RSM technique models were first compared for predicting capacity for Cr(VI) uptake by CoAl-LDH and bentonite-CoAl-LDH from water based on FC-CCD data, which forms the

basis of the RSM modeling. Traditionally, this has been the approach adopted in similar reported adsorption studies for comparing the performance of ANN and RSM techniques. In addition, this present work further uniquely provides a comparative assessment of the performance of the developed ANN and RSM models for the mechanistic aspects of Cr(VI) uptake behaviors onto the LDHs from water.

2. Materials and Methods

2.1. Materials, Synthesis, and Characterizations of LDHs

High purity aluminum ($Al(NO_3)_3 \cdot 9H_2O$, 98%) and cobalt nitrate ($Co(NO_3)_2 \cdot 6H_2O$, 97%) salts and bentonite (powdered commercial BDH, UK) 2.5 g/cm^3 density were the main reagents used for the CoAl-LDH and bentonite-CoAl-LDH syntheses. Sodium hydroxide (NaOH, 99%) and nitric acid (HNO_3, 99%) were purchased from Sigma–Aldrich Co., St. Louis, MO, USA. Similarly, all other high purity reagent chemicals used were acquired from Sigma–Aldrich Co., USA. Deionized water (DI) produced from the laboratory with a Millipore-Ultrapure water treatment device was used for preparation of 1000 mg/L stock solution of Cr(VI), dilution as well as other purposes during the entire the study.

The bentonite-CoAl-LDH was synthesized via intercalation of bentonite particles into the synthesized parent CoAl-LDH. For both adsorbents, the coprecipitation method was employed for their synthesis as per our earlier works [18,25]. For the synthesis, 60 mL of water containing mixture of 30 mmole $Co(NO_3)_2 \cdot 6H_2O$ and 10 mmole $Al(NO_3)_3 \cdot 9H_2O$ in 0.5 L round bottom flask was vigorously stirred for 15 min at 600 rpm and 60 °C. Afterwards, 1 M NaOH was introduced into the flask via dropwise addition to achieve pH of 10. The next step involved stirring the mixture at 1000 rpm, temperature of 90 °C and refluxing of the slurry for one day. Thereafter, centrifuging the resulting mixture was carried out and two step prior final washing with ethanol produced a denser slurry that was subjected to one day 90 °C vacuum oven drying to obtain the finished CoAl-LDH product. Meanwhile, for the synthesis of the bentonite-CoAl-LDH composite, prior to the described Co-Al-LDH salt-co-precipitation procedure above, bentonite (about 0.5 g) was added to the 60 mL DI and subjected to ultrasonicated at 60 rpm for 30 min. Characterization of the produced adsorbent was undertaken using Brunauer Emmett Teller (BET, Micromeritics, Tristar II series, UK), scanning electron microscopy (SEM, SM-6460LV (Jeol, Tokyo, Japan)) and transmission electron microscopy TEM (TEM, FEI Morgagni 268, Czech Republic).

2.2. Characterization and Analysis Methods

Analyses of the physico–chemical characteristics of the LDHs were achieved using the following instruments: Nicolet 6700 Fourier transform-IR (FTIR, Thermo Fisher Scientific, Waltham, MA, USA) with resolution 4 cm^{-1}; D8 advanced X-ray instrument for X-ray diffraction (XRD) at 2θ = 70° to 2° and 0.1542 nm wavelength and Brunauer Emmett Teller analysis (BET, Micromeritics, Tristar II, Norcross, GA, USA) and SM-6460LV (Jeol, Japan) scanning electron microscopy (SEM)

2.3. Cr(VI) Adsorption onto CoAl-LDH and Bentonite-CoAl from Aqueous Phase Tests

2.3.1. FC-CCD Study

The RSM modeling was implemented based on the FC-CCD experimental design. The FC-CCD consists of 3 k, 2 k and k, respectively, representing factorial runs, axial runs and replicated central runs, with schematic design space represented in Figure 1b (where k = number of independent variable) [6]. The merits of adopting the FC-CCD over other forms of the CCD include (i) the central position with star points at each factorial space (i.e., $\alpha = \pm 1$); (ii) it requires fewer levels of each factor (3 against 5 for other designs) and (iii) it can incorporate resolution V or full factorial design with appropriate star points [27]. In this study, a 3^3 FC-CCD was adopted which involves three independent variables: A (temperature), B (initial Cr(VI) concentration) and C (initial pH). These are presented in Table 1 with ranges and values, and a fixed contact time of 180 min for all experiments was chosen according to preliminary experiments and our previously published work [18]. The

initial Cr(VI) solution pH value was adjusted to the required value for each experiment using 0.1 M NaOH and 0.1 M HNO_3 and solutions. Accordingly, seventeen (17) randomized duplicated tests with three central run replicates (to estimate error and the response surface curvature) [6,27] were undertaken (Table 2). At the end of each test, the sample was first filtered using 0.45 µm cellulose acetate filters followed by centrifugation for 5 min at 4000 rpm for 5 min and the residual Cr(VI) concentration was analyzed using ICP-OES (Horiba, Irvine, CA, USA). The two targeted responses (dependent variables) in this study are the CoAl-LDH (Qe1) and bentonite-CoAl-LDH (Qe2) uptake capacity for Cr(V) uptake from water which were estimated using Equations (1).

$$\text{Qe1 or Qe2} = \frac{C_o - C_e}{W} * V \quad (1)$$

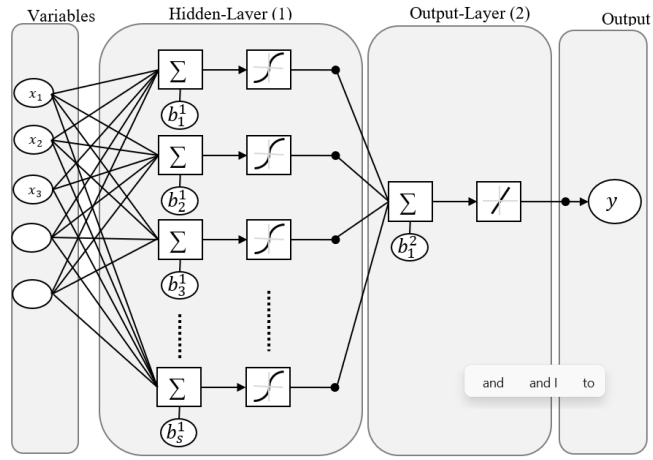

(**a**)

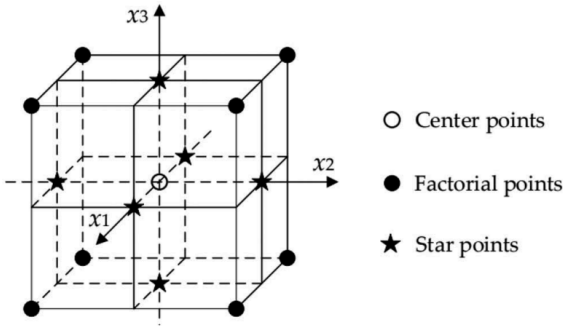

(**b**)

Figure 1. Schematic representation of (**a**) ANN and (**b**) 3-factor 3-level RSM-FC-CCD.

Table 1. Cr(V) uptake for FC-CCD experimental design space.

	Experimental Variables	Levels		
		High-Lower (+1)	**Mid-Level (0)**	**Lower Level (−1)**
A	Temperature (°C)	45	35	25
B	Initial Cr(IV) conc. (mg/L)	127	76.5	26
C	Initial pH	6	4	2

Table 2. FC-CCD experimental variables and results for CoAl-LDH (Qe1) and bentonite-CoAl-LDH (Qe2).

Standard Order	Run Order	A: Temperature °C	B: Inital Cr(VI) Conc. mg/L	C: Initial pH	Qe1, mg/g	Qe2 mg/g
16	1	35	76.5	4	38.10	51.36
4	2	45	127	2	58.32	63.92
3	3	25	127	2	77.44	101.36
2	4	45	26	2	18.80	20.4
14	5	35	76.5	6	43.20	43.44
7	6	25	127	6	43.60	55.76
17	7	35	76.5	4	36.99	53.212
8	8	45	127	6	36.40	45.76
15	9	35	76.5	4	37.44	52.48
11	10	35	26	4	19.60	25.84
13	11	35	76.5	2	45.44	58.4
12	12	35	127	4	44.48	75.12
1	13	25	26	2	35.92	34.8
5	14	25	26	6	19.12	19.84
10	15	45	76.5	4	76.88	30.64
9	16	25	76.5	4	63.04	71.44
6	17	45	26	6	19.68	15.52

2.3.2. Kinetics and Thermodynamics Study

Using similar experimental procedure as for the FC-CCD tests explained above, a complete thermodynamics study was undertaken at different operating conditions. Thermodynamics experiments were conducted at temperature (25, 35 and 45 °C); initial pH (2, 4 and 6) and initial Cr(VI) concentration (49.58, 76.5 and 107.69) mg/L. Meanwhile, the kinetics experiments were conducted at fixed temperature 25 °C; initial pH 2 and initial Cr(VI) concentration (20, 60 and 100 mg/L). Additionally, an adsorbent dosage of 5 mg in 40 mL samples was used.

2.4. Math Techniques and Performance Evaluation

2.4.1. RSM Experiments and Modeling

RSM modeling: The RSM generalized second order polynomial function given in Equation (2) was used for RSM models fitting for Qe1 and Qe2 using Design Expert 8.0 statistical program.

$$\text{Qe1 or Qe2} = \beta_0 + \sum_{i=1}^{k} \beta_i x_i + \sum_{i=1}^{k} \beta_i x_i^2 + \sum_{i=1}^{k-1} \sum_{j=2}^{k} \beta_{ij} x_i x_j + \varepsilon \quad (2)$$

where, C_o = initial and C_e = equilibrium Cr(VI) concentration in mg/L, Qe1 or Qe2 predicted uptake capacity for Cr(V) uptake from water for the tested LDH in mg/g, β_{ii}, β_{ij}, $\beta_{i,}$ β_0, are the developed q_e model's coefficients; x_i and x_j, = operational conditions.

2.4.2. Artificial Neural Network (ANN) Models Development

The ANN modeling for the Qe1 (CoAl-LDH) and Qe2 (bentonite-CoAl-LDH) data was undertaken using MatLabTM (R2017a) ANN framework for data fitting with general architectural structure presented in Figure 1a. The steps involve splitting each of the input data (Qe1 or Qe2) into training (70%), validation (15%) and test (15%) data; selection of hidden layer followed by selection of ANN based algorithms prior to running the model. The ANN algorithms employed to obtain the best data representation included scaled conjugate gradient (SCG), Bayesian Regularization (BRA) and the Leverberg–Marquartz algorithm (LMA) as per earlier reported works [2,12].

2.4.3. Developed Models' Performance Evaluation

The Qe1 and Qe2 prediction quality of the developed ANN and RSM-FC-CCD models were assessed and compared as per coefficient of determination R^2 and RMSE (lower values desired)-based Equations (3) and (4), respectively.

$$R^2 = 1 - \frac{(y_i - \acute{y}_i)^2}{(y_i - \overline{y})^2} = 1 - \frac{SSR}{SST} \quad (3)$$

$$\text{RMSE} = \frac{1}{n}\sum_{i=1}^{n}(y_i - \acute{y}_i)^2 = \frac{1}{n}\sum_{i=1}^{n} SST \quad (4)$$

where y_i = actual value, $\overline{y}$ = mean value, $\acute{y}_i$ = predicted value, SSR = residuals sum of squares and SST = total sum of squares

3. Results and Discussion

3.1. Adsorbent Characterization Analysis

The SEM images of the raw bentonite, CoAl-LDH, as well as their resulting intercalated composites are presented in Figure 2. Figure 2b,c shows that the particles of CoAl-LDH and bentonite-CoAl-LDH adsorbents are homogeneous and rough with the latter being more uniform and porous in nature [25]. This slight disparity could be attributed to the presence of the intercalated particles of bentonite in the bentonite-CoAl-LDH which suggests a successful incorporation of the bentonite particles in the original LDH. The SEM image in Figure 2c also shows that there is uniform dispersion of bentonite-CoAl-LDH within the bentonite interlayers [18].

Figure 3b shows the FTIR spectra of bentonite-CoAl-LDH adsorbent. When compared to the spectra of CoAl-LDH in Figure 1a, it can be seen that there is a clear stretching vibration at 1000 cm^{-1} which can be assigned to the bond involving Si-O-Al bond resulting from the incorporation of bentonite in the bentonite-CoAl-LDH adsorbent [28]. Interestingly, the characteristic patterns of CoAl-LDH and raw bentonite are manifested in the B-CoAl composite, indicating strong integration of bentonite into the parent CoAl-LDH. This is further confirmed by the EDS elemental analysis given in Table 3. For both adsorbents, the clear peaks located at 3000 and 3500 cm^{-1} are assigned to the interlayer molecules of stretching vibrations O-H and C-H groups [29]. Moreover, the carbonyl group bending vibration are observable at 1750 cm^{-1} for both adsorbents while the nitrate ion interlayer symmetric stretching appears at 1358 cm^{-1}. The peak between 1001 cm^{-1} and 1217 cm^{-1} can be attributed to the C-O-C and C-O group [30]. Meanwhile, the stretching vibrations observed below 1000 cm^{-1} can be are ascribed to the presence of oxygen–metal–oxygen, metal-o-metal, brucite-type, Al-O and Co-O [28]. Moreover, the slight variability in the peaks between the two adsorbents was attributed to the relative quantity of the bentonite used in the production of the composite samples. The XRD results presented in Figure 4 indicates peaks at the 113, 110, 018, 012 planes which are ascribed to 61.1°, 59.8°, 44.9° and 36.9°, respectively, [18]. Meanwhile, the basal spacing of d006 and d003 are located at the 23.0° and 11.4°, respectively. The bentonite-CoAl-LDH XRD result (Figure 4c) reaffirmed the characteristics of the parent CoAl-LDH (Figure 4b) with minimal reduction in the basal spacing. After the incorporation of bentonite into the LDH, the bentonite-CoAl-LDH maintains the reflections of CoAl-LDH but with slight reduction in the d006 and d003 diffraction peaks. Meanwhile both the parent and resulting bentonite intercalated composite shows improved diffraction intensity suggesting a crystallinity of good quality [31].

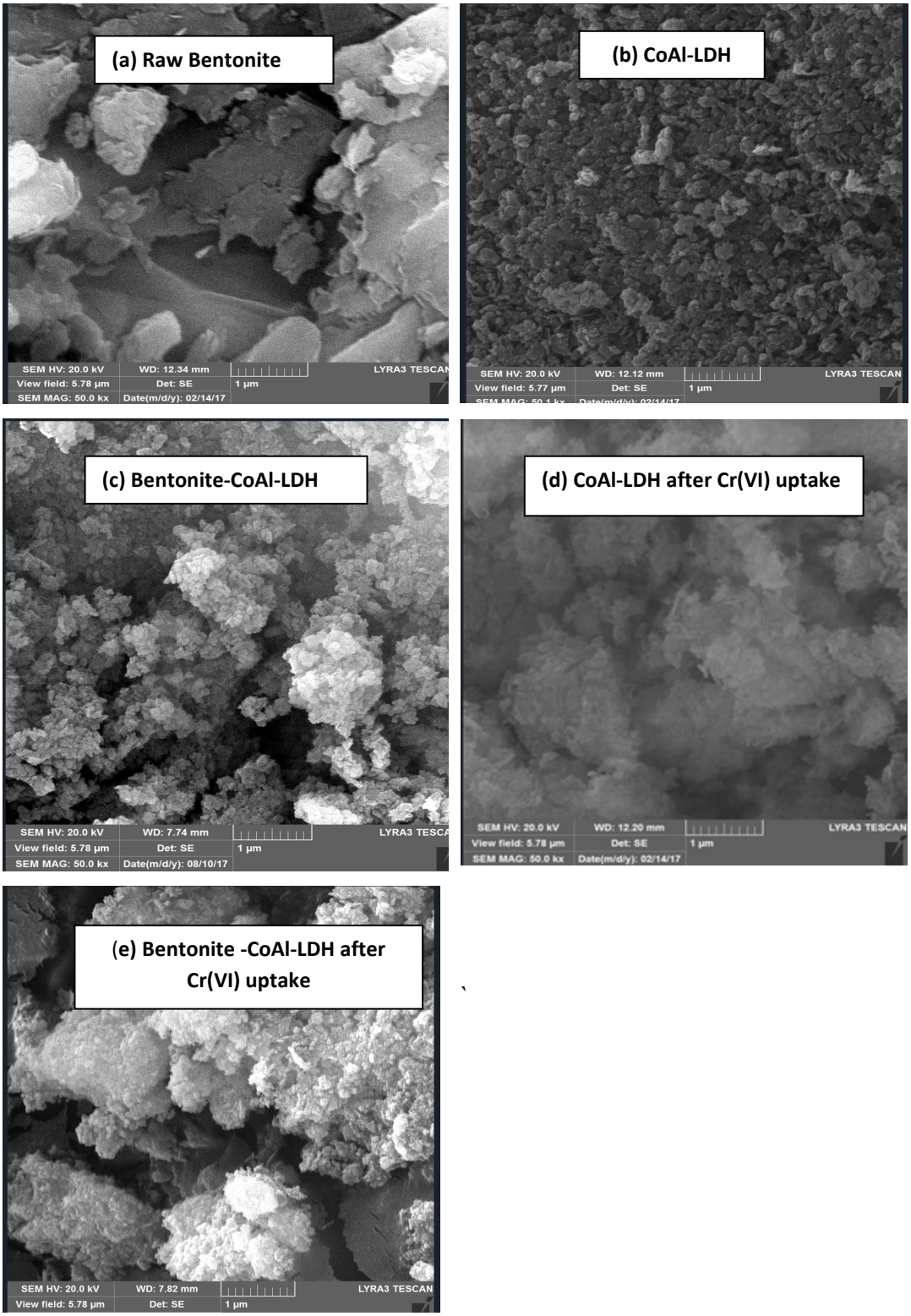

Figure 2. SEM image of raw bentonite (**a**); CoAl-LDH before Cr(VI) uptake (**b**); bentonite-CoAl-LDH before Cr(VI) uptake (**c**); CoAl-LDH after Cr(VI) uptake (**d**) and bentonite-CoAl-LDH after Cr(VI) uptake (**e**) under optimal adsorption conditions of temperature = 25 °C, pH 2 and 126 mg/L initial Cr(VI) concentration.

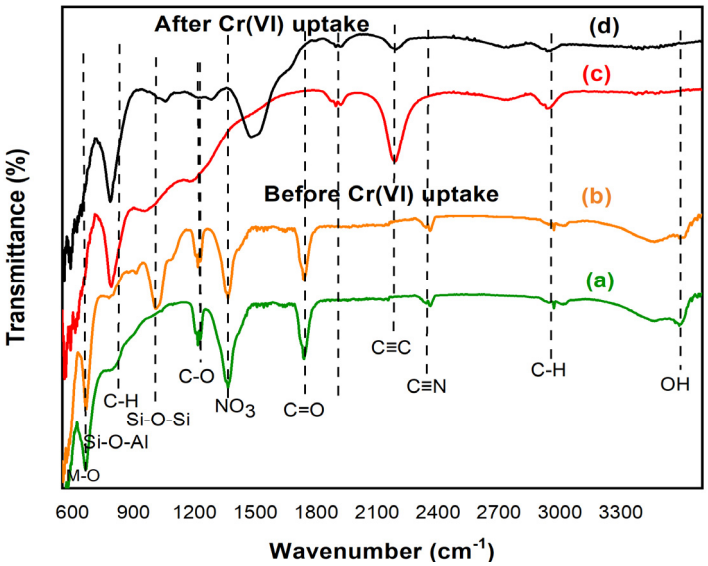

Figure 3. FTIR of CoAl-LDH before Cr(VI) uptake (a); bentonite-CoAl-LDH before Cr(VI) uptake (b); CoAl-LDH after Cr(VI) uptake (c); bentonite-CoAl-LDH after Cr(VI) uptake (d) under optimal conditions of temperature = 25 °C, pH 2 and 126 mg/L initial Cr(VI) concentration.

Table 3. EDS elemental analysis for raw bentonite and the adsorbents.

Raw Bentonite		CoAl-LDH		Bentonite-CoAl-LDH	
Element	**Weight %**	**Element**	**Weight %**	**Element**	**Weight %**
C	13.87	O	24.69	C	8.68
O	51.83	Al	5.72	O	39.12
Na	1.16	Co	69.59	Al	6.54
Mg	1.33	-	-	Si	2.64
Al	7.47			Co	40.36
Si	18.22	-	-	Cu	2.66
Cl	1.06			-	-
Ca	0.56	-	-		
Fe	2.66			-	-
Cu	1.85	-	-		
Totals	100.00	-	100	-	100

After the Cr(VI) adsorption process, the FTIR characteristic peak patterns for CoAl-LDH (Figure 3c) and bentonite-CoAl-LDH (Figure 3d) completely changed, indicating successful uptake of the Cr(VI) molecules [18]. SEM images in Figure 2d,e which represent the morphology of the adsorbents after the uptake of Cr(VI) show a visible change in morphology of the adsorbents when compared to the images before Cr(VI) uptake. This suggests successful integration of the Cr(VI) onto the active binding sites of the adsorbents. This further supports the observations in the FTIR peaks in Figure 3c,d that shows conspicuous alteration after the Cr(VI) uptake. For example, there is a clear reduction in C-O associated groups located at 1001 cm^{-1} aftermath of the Cr(VI) uptake. Other peaks, especially those that were observed prior to the Cr(VI) uptake, were nearly eliminated. This included the sharp peaks at 3446 cm^{-1} (related to OH), 1650–1780 cm^{-1} (related to C=O) and 1340–1360 cm^{-1}(related to −COO) (Figure 3a), corroborating the SEM results. In general, these observations suggest a successful attraction of the Cr(VI) onto the adsorbents binding sites via electrostatic, covalent and hydrogen bonding between various observed surface functional groups and the molecules of the metal ions.

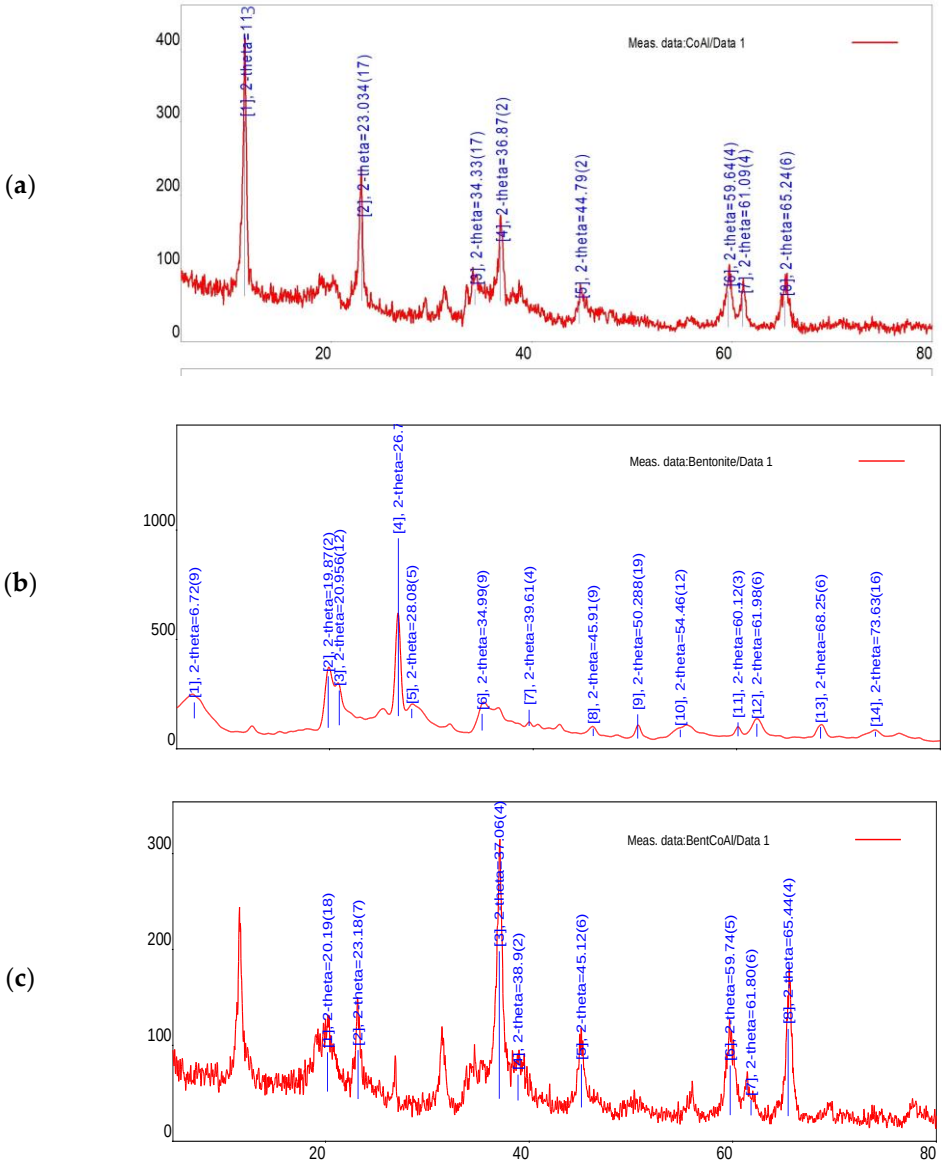

Figure 4. XRD for (**a**) raw bentonite (**b**) CoAl-LDH and (**c**) bentonite-CoAl-LDH.

The thermal stability of the bentonite-CoAl-LDH adsorbent was investigated using TGA analysis between temperature range of 20–800 °C as presented elsewhere [9]. The result indicates adsorbent weight loss of around 20–23% between 20 to 200 °C. This observation can be attributed to the initial loss of bounded water molecules. When the temperature was increased to 300 °C, observed weight losses were around 54%, suggesting a good thermal stability under higher temperature beyond the operational temperatures of the adsorption tests.

Under a nitrogen atmosphere, the adsorption–desorption isotherm was employed to obtained pore characteristics, which suggests a H3-type hysteresis loop as recognizable as at type IV isotherm at 1.0-0.05P/P0 [18]. The diameter of the bentonite-CoAl-LDH pores (1.95 nm) indicates their mesoporous nature and also suggests the presence of micropores on its surface. Meanwhile, the BET areas for CoAl-LDH and bentonite-CoAl-LDH were obtained as 44 m^2/g, 119 m^2/g, respectively. The significant increase in surface BET area of the bentonite-CoAl-LDH composite further establishes the efficacy of bentonite intercalation using the co-precipitation method. In conclusion, these results reaffirm success in production of the composite material via the adopted bentonite procedure and the high

potential of the two LDHs materials as good adsorbents for heavy metal remediation in contaminated water

3.2. Cr(VI) RSM Sorption Model Development and Evaluation

3.2.1. Cr(VI) Sorption RSM Model Development

Table 2 presents the obtained data from the batch adsorption test. Each uptake capacity Qe is the average value for the two duplicated adsorption data obtained. The values for the uptake capacity of Cr(VI) for CoAl-LDH and its bentonite modified version ranged between 18.80 to 77.44 mg/g and 15.52 to 101.36 mg/g, respectively. This implies a significant increase in the uptake capacity as result of interaction of the raw bentonite with the parent LDH [25]. Design Expert® aided regression analyses were employed for fitting the data in Table 2 into Equation (2) for the development of RSM models. As per the high models' term significance having no alias (Table 4) [6], the best RSM models were found to be quartic functions given in Equations (5) and (6). Only the reduced models (Table 4 ANOVA significant terms on respective response i.e., p-values < 0.05) are included [6]. However, some terms were insignificant in the bentonite-CoAl-LDH model, but when interacted with other terms, they generated higher terms that became significant. Therefore, the lower terms were left in the model to satisfy hierarchical effects as required by RSM [6]. Table 4 shows that all the single terms A, B and C (the single effects), BC, AB, AC (2-way interaction effects), squared terms A^2, B^2 and C^2, cubic term ABC, A^2B, A^2C and AB^2 as well as quartic term A^2B^2 are significant model terms.

$$\begin{aligned}\text{Qe1 (Uptake capacity for CoAl-LDH)} = 37.51 + 6.92A + 12.44B - 1.12C - \\ 1.22AB + 3.70AC - 4.98BC + 32.45A^2 - 5.47B^2 + 6.81C^2 - 0.7200ABC + 2.84A^2B \\ - 7.84A^2C - 12.28AB^2 - 32.64A^2B^2\end{aligned} \quad (5)$$

$$\begin{aligned}\text{Qe2 (Uptake capacity for Bentonite-CoAl-LDH)} = 52.35 - 20.40A + 24.64B - \\ 9.86C - 3.59AB + 4.69AC - 5.49BC - 1.31A^2 - 1.87B^2 - 1.43C^2 - 2.61A^2B + \\ 12.13AB^2 - 3.07A^2B^2\end{aligned} \quad (6)$$

Table 4. ANOVA for CoAl-LDH and bentonite-CoAl-LDH RSM models.

Qe1			Qe2		
Source	**F-Value**	***p*-Value**	**Source**	**F-Value**	***p*-Value**
Model	1236.10	0.0008	Model	50.82	0.0009
A	307.26	0.0032	A	62.20	0.0014
B	992.97	0.0010	B	90.74	0.0007
C	8.05	0.1050	C	72.60	0.0010
AB	38.20	0.0252	AB	7.71	0.0500
AC	351.36	0.0028	AC	13.15	0.0222
BC	636.52	0.0016	BC	18.02	0.0132
A^2	4053.91	0.0002	A^2	0.1541	0.7147
B^2	115.19	0.0086	B^2	0.3138	0.6052
C^2	178.54	0.0056	C^2	0.1836	0.6904
ABC	13.31	0.0676	A^2B	0.8145	0.4178
A^2B	41.40	0.0233	AB^2	17.59	0.0138
A^2C	315.51	0.0032	A^2B^2	0.2379	0.6513
AB^2	774.07	0.0013			
A^2B^2	1155.36	0.0009			

3.2.2. Cr(VI) Adsorption Pareto Charts

The main effects and the two-way interaction proportional contributions (hierarchical influence) assessment on the sorption capacity in the form of Pareto charts are represented in Figure 5a,b for the tested adsorbents. Accordingly, the Pareto's plot height proportionally indicates the relative importance of the parameters on the Qe1 and Qe2 responses; the high bar reflects higher significant influence and the low bar reflects otherwise [9]. Consequently,

factors B and C mainly controlled the uptake capacity of Cr(VI) onto CoAl-LDH adsorbents (Figure 5a). However, Figure 5b shows that factors B, A and C mainly controlled the uptake capacity of Cr(VI) onto bentonite-CoAl-LDH.

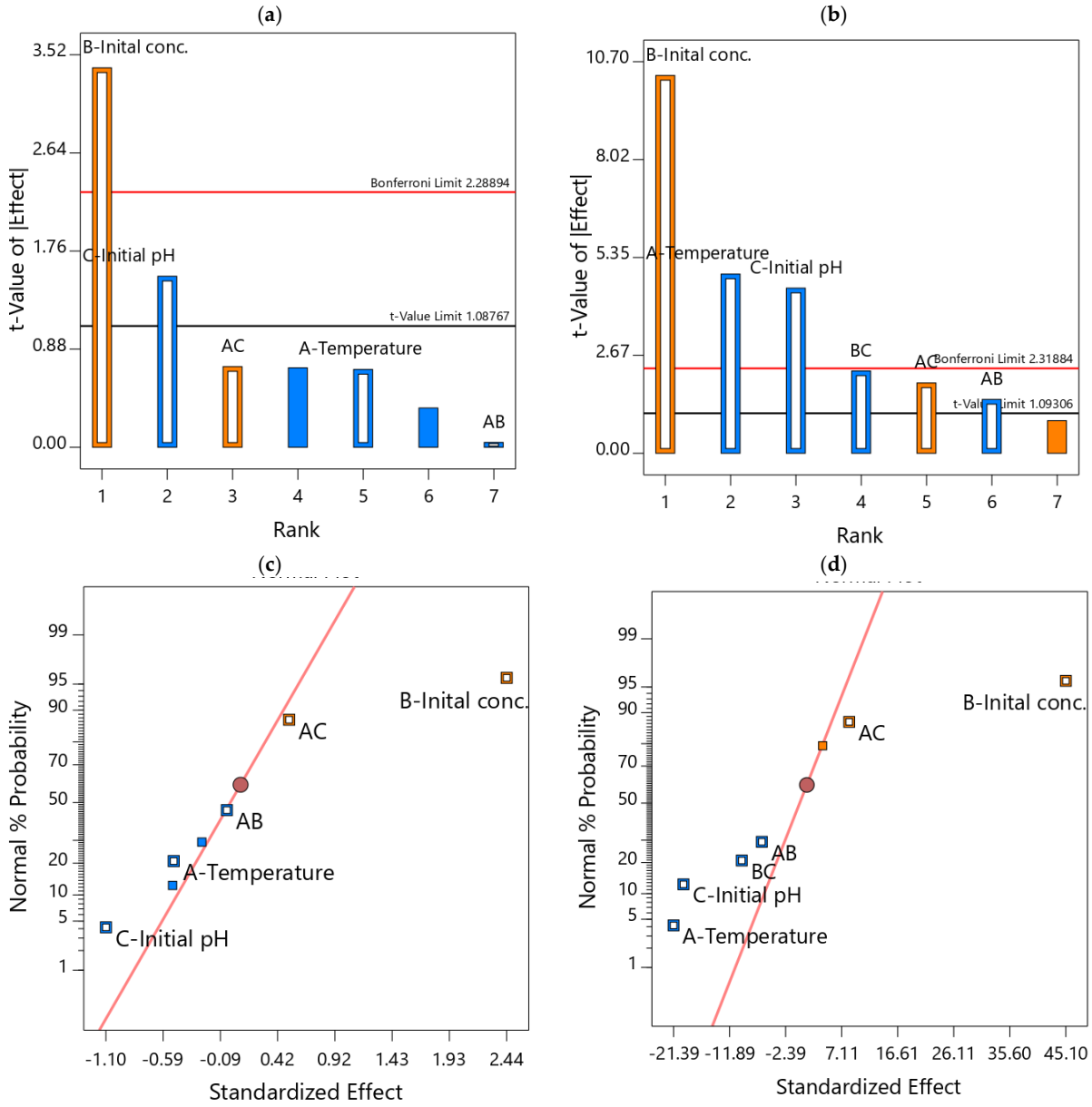

Figure 5. Pareto diagrams (**a**,**b**) and probability normal plots (**c**,**d**) the influence of independent variables on Qe1 and Qe2 for Cr(VI) removal from water, respectively.

3.2.3. Cr(VI) Adsorption RSM Model Validation

The coefficients of determination (R^2), of the developed and tested LDHs sorption models are 0.9999, 0.9935 for Qe1 and Qe2, respectively. Moreover, both the R^2 adjusted and predicted are close to the main R^2, indicating the high quality of the models and their capability for prediction of the test data as demonstrated by the lower residuals (mostly zero) in Table 5. The plots of normal probability presented in Figure 5c,d are linear, indicating normally distributed experimental data [6].

Table 5. RSM models predictions for FC-CCD tests data for Cr(VI) uptake capacity Qe1 and Qe2.

	CoAl-LDH (Qe1)			Bentonite-CoAl-LDH (Qe2)		
Run Order	**Actual Value**	**Predicted Value**	**Residual**	**Actual Value**	**Predicted Value**	**Residual**
1	38.10	37.51	0.5900	51.36	52.35	−0.9907
2	58.32	58.32	0.0000	63.92	65.50	−1.58
3	77.44	77.44	0.0000	101.36	98.60	2.76
4	18.80	18.80	0.0000	20.40	17.64	2.76
5	43.20	43.20	0.0000	43.44	41.06	2.38
6	43.60	43.60	0.0000	55.76	58.52	−2.76
7	36.99	37.51	−0.5200	53.21	52.35	0.8613
8	36.40	36.40	0.0000	45.76	44.18	1.58
9	37.44	37.51	−0.0700	52.48	52.35	0.1293
10	19.60	19.60	0.0000	25.84	25.84	0.0000
11	45.44	45.44	0.0000	58.40	60.78	−2.38
12	44.48	44.48	0.0000	75.12	75.12	0.0000
13	35.92	35.92	0.0000	34.80	36.38	−1.58
14	19.12	19.12	0.0000	19.84	18.26	1.58
15	76.88	76.88	0.0000	30.64	30.64	0.0000
16	63.04	63.04	0.0000	71.44	71.44	0.0000
17	19.68	19.68	0.0000	15.52	18.28	−2.76

3.3. Cr(VI) Uptake Capacity Operational Parameter Influence and Optimization

Figures 6 and 7 present the 3D and contour representation of effects of operational variables on the CoAl-LDH and bentonite-CoAl-LDH adsorption capacities for Cr(VI) removal from water, respectively. Figures 6a,b and 7a,b reveal that the Cr(VI) uptake capacity increased when initial concentration was increased, and pH was decreased for both adsorbents. The uptake capacity for both adsorbents was found to predominantly improve with a decrease in temperature (Figures 6b,c and reffig:water-1708317-f007b,c), signifying a sorption process that is exothermic in nature (confirmed by thermodynamics data under Section 3.5.2, which is in conformity with results from other reported studies [18,32,33]. For the bentonite-CoAl-LDH, the highest uptake capacity for Cr(VI) was improved by a factor of 6.5 and 4.1 to 77.44 and 101.36 mg/g when the Cr(VI) concentration was increased from 26–127 mg/L. At a given adsorbent dosage, the observed positive influence of increase in the initial concentration on the enhancement of the uptake capacity of the adsorbents was attributed to an increase in potentials of better relations between the increased Cr(VI) ions with the abundant active sorption sites [34,35].

At fixed initial concentration of 127 mg/L and temperature of 25 °C (Table 2), the uptake capacity of Cr(VI) significantly reduced from 77.44 to 43.6 mg/g and from 101.36 mg/g to 55.76 mg/g for CoAl-LDH and bentonite-CoAl-LDH, respectively, when the initial pH was raised from 2 to 6. This is similar for other operational conditions which clearly suggest a decline in the uptake capacity of the tested adsorbents with increases in pH (Figures 6 and 7), which can be attributed to the changes in the adsorbent surface charge characteristics resulting from the pH variability. Within the acidic pH range of 2–6, Cr(VI) ions is in its anionic forms $Cr_2O_7^{2-}$, $Cr_2O_4^{2-}$ and $HCrO^{4-}$ in the aqueous phase [36,37].

The point of zero charge (pH_{pzc}) found from the drift method for CoAl-LDH and bentonite-CoAl-LDH was found to be 4.84 and 5.15 [18], respectively. This indicates that achieving a higher state of surface protonation for both adsorbents was expected to have occurred when the pH was lower (i.e., pH 2), thereby causing stronger adsorbent–adsorbate electrostatic attraction, and thus explaining the observed high uptake capacity for Cr(VI) ions at such pH. Thus, by raising the pH from the lowest to the highest level, it means that additional HO^- ions were introduced that were susceptible to deprotonate the adsorbent surfaces while competing with the predominantly existing anionic forms of Cr(VI), thereby exhibiting the decline in the uptake capacity with increasing pH for both adsorbents. The observed improved performance for the bentonite-CoAl-LDH composite is attributed to its

improved physico–chemical characteristics compared to the parent LDH as discussed in Section 3.1.

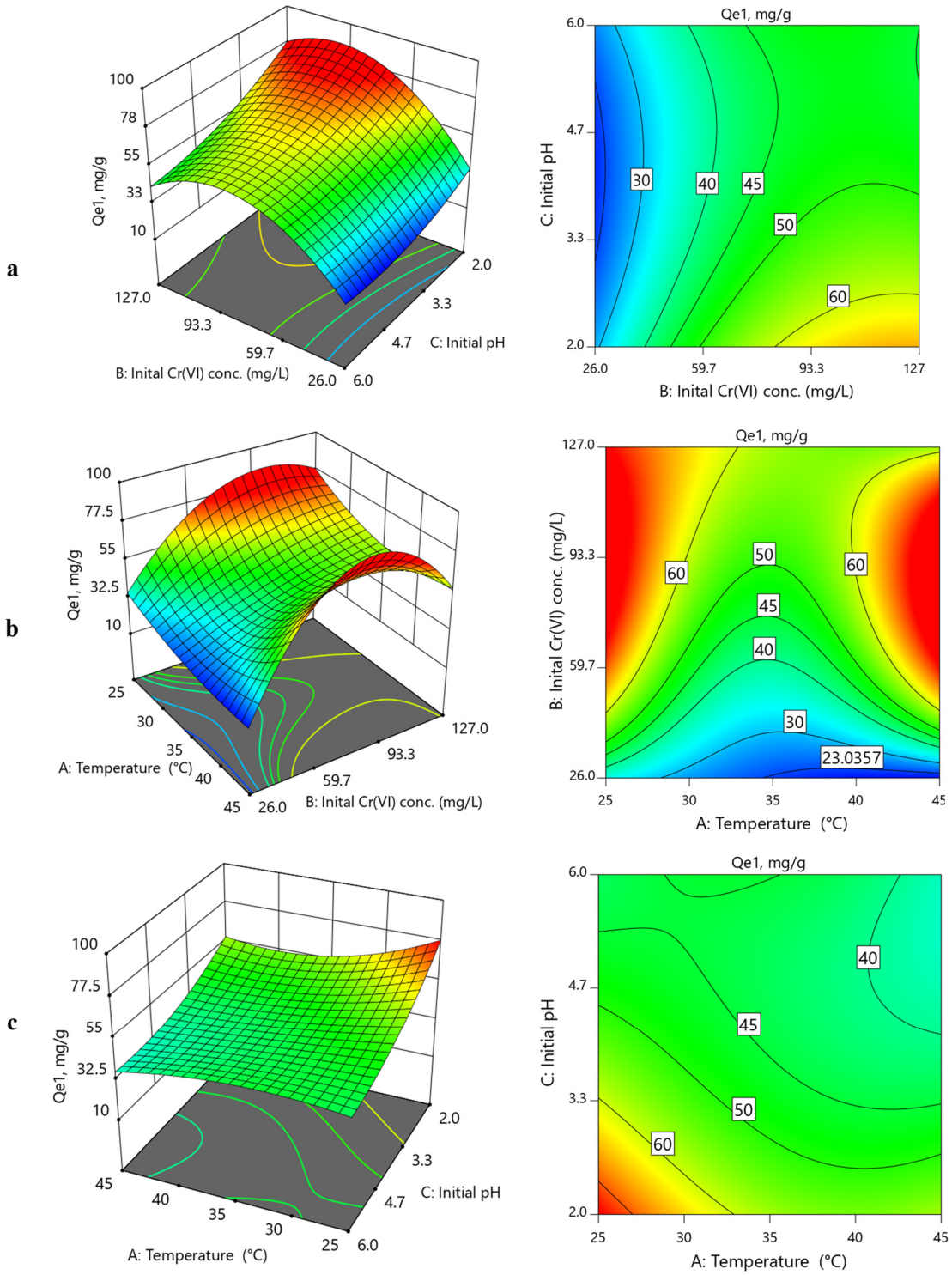

Figure 6. 3D and 2D contour plots for binary influence of (**a**) initial Cr(VI) concentration vs. initial pH; (**b**) temperature vs. initial Cr(VI) concentration; (**c**) initial pH vs. temperature on CoAl-LDH uptake capacity (Qe1) for Cr(VI) removal from water.

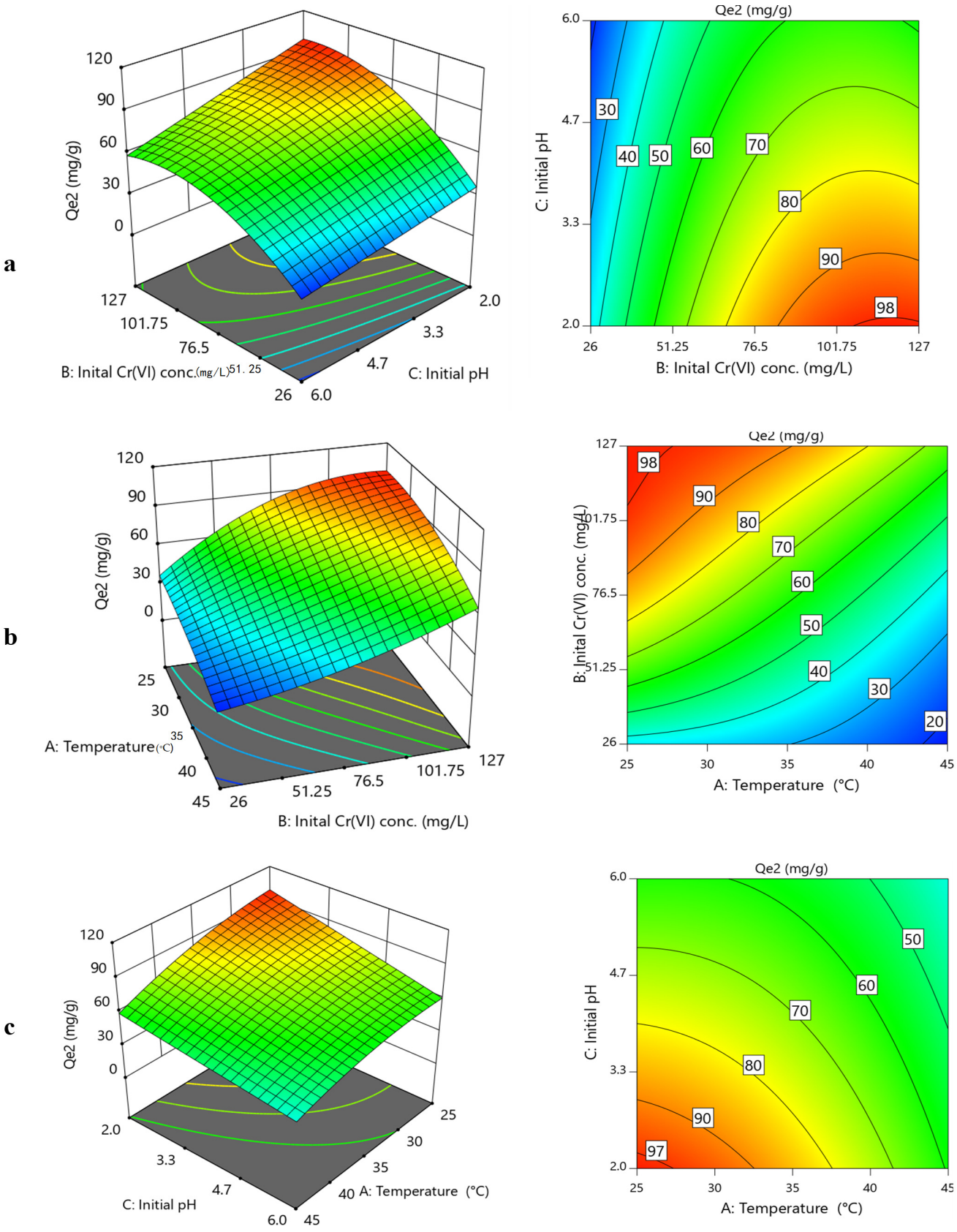

Figure 7. 3D and 2D contour plots for binary influence of (**a**) initial Cr(VI) concentration vs. initial pH; (**b**) temperature vs. initial Cr(VI) concentration; (**c**) initial pH vs. temperature on bentonite-CoAl-LDH uptake capacity (Qe2) for Cr(VI) removal from water.

The numerical solutions of optimal operation conditions for the best Cr(VI) removal were studied based on desirability functions. The results showing the interactive influences of operational parameters are presented in Table S1 and visually depicted in Figure 8 as desirability of conditions in maximizing uptake capacity for Cr(VI) for finding optimal solutions. The trends indicate that Cr (VI) uptake capacity improved with increasing Cr(VI) initial concentration and initial pH, while increasing the operational temperature was susceptible to decrease the adsorption capacity. The most durable optimal operating parameters provides initial pH = 2, temperature = 25 °C and initial Cr(VI) concentration of 126 mg/L as the best conditions.

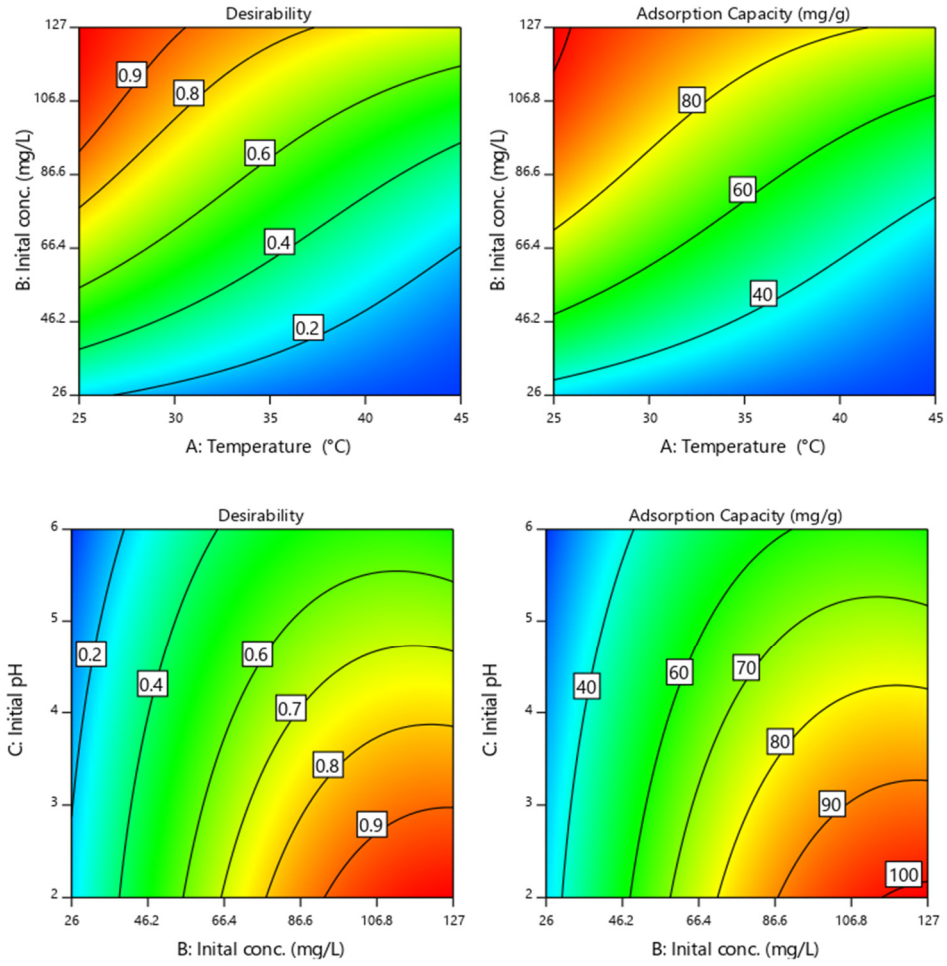

Figure 8. Desirability conditions for maximizing uptake capacity for Cr(VI) removal from water and finding optimal solutions.

3.4. Cr(VI) ANN Uptake Modeling and Optimization Strategy

The experimental data provided in Table 2, Tables S1 and S2 for RSM-FC-CCD, equilibrium and kinetics studies were used to develop the ANN models using SCG, BRA and LMA algorithms within the MatLabTM (R2017a) neural network fitting framework. For each experiment scenario, the ANN predictive Cr(VI) uptake model for CoAl-LDH bentonite-CoAl-LDH (designated as Qe1 and Qe2, respectively) were developed. Accordingly, the ANN-based algorithms (SCG, BRA and LMA) were employed for developing the best ANN models by varying the number of neurons from which the optimal number of neurons that yielded the best performances were arrived at after several comparative trials. Preliminary evaluations indicated the suitability of the LMA algorithm for both Qe1 and Qe2 based on its consistent excellent predictive performance. Thus, the LMA was adopted for the final training as well as optimizing all the ANN models. The ANN-LMA models' optimization

was also experimented by changing the neuron numbers for further increasing R^2 to achieve values close to unity while ensuring that RMSE values were significantly reduced for the training, validation and the overall data sets.

For each of the ANN-LMA cases, the best tested epoch and number of neurons were adjusted until the optimal solutions for Qe1 and Qe2 were achieved as depicted in Figure 9. The ANN-LMA model optimization strategy for FC-CCD, thermodynamics and kinetics for Cr(V) capacity, Qe1 and Qe2 are provided in Figure 9a–e, respectively. The parameters (training, testing, validation and overall R^2 and RMSE, neuron numbers are epoch) developed from the ANN-LMA model performance for predicting the various Cr(VI) uptake onto the tested adsorbents are presented in Table 6. Interestingly, the predominance of lower RMSE for Qe1 (3.092, 4.089 and 17.32) and Qe2 (2.982, 4.99 and 6.75) and corresponding higher values of overall R^2 for training (0.995–0.999), validation (0.905–0.999), testing (0.903–0.995) and overall (0.993–0.999) show high predictive ability of the developed ANN-LMA models.

3.5. ANN vs. RSM Cr(VI) Adsorption Models' Comparative Performance

ANN and RSM modeling techniques have become increasingly desirable mathematical techniques that are adopted for understanding environmental processes such as remediation of water and wastewater using adsorption [1,2,26]. Recently, researchers have been devoting significant efforts to understating the best of the two approaches via comparing the ability of these two approaches in providing dependencies of target responses on operational parameters of various adsorption processes [9,38,39]. However, reported works on predictive modeling of adsorption onto LDHs have mainly focused on RSM techniques with rare studies reported on the applicability of ANN models for heavy metals removal from water [26]. Recently, Zhu et al. [26] reported the ANN predictive performance of Cr(VI) ions' uptake onto LDH nanocomposite of organic framework from which excellent predictions were obtained. However, such studies have been short of investigating the potentials of predicting adsorption kinetic and thermodynamic behaviors. In the present study, ANN-LMA and RSM-based adsorptive models were firstly compared for predicting capacity for Cr(VI) uptake by CoAl-LDH and bentonite-CoAl-LDH from water based on FC-CCD experimental results. As explained earlier, these sets of experimental data were mainly employed to develop the RSM models based on fitting data in Table 2 using Equation 2. Traditionally, this has been the approach adopted in earlier reported adsorption studies for comparing the performance of ANN and RSM techniques [9,40,41]. However, as an improvement on this approach, the present study further investigated the ANN-LMA and RSM-based models for predicting thermodynamic and kinetic behaviors taking into account additional experiments that are completely different from the FC-CCD, though within the FC-CCD experimental design space. This is necessary, owing to the fact the RSM model predictions are restricted to operate within such limited bound. The results obtained are assessed, compared, and discussed in the respective subsections below.

3.5.1. ANN and RSM Prediction of FC-CCD Data for LDHs Cr(VI) Uptake

The developed ANN-LMA and RSM model predictive fitting parameters for the FC-CCD Cr(VI) uptake onto CoAl-LDH and bentonite-CoAl-LDH from water (designated as Qe1 and Qe2, respectively) are given in Table 6 while predicted vs. experimental data are presented in Figure 10. The R^2 for the RSM models of 0.999 and 0.998 are slightly higher, yet quite comparable to those of the ANN-LMA (0.995 and 0.997). However, lower RMSE values for RSM (0.195 and 1.774) suggest a higher predictive performance of the RSM models over the ANN-LMA (3.092 and 2.982). Although the better RSM performance cannot be fully justified considering that ANN-LMA models were more restrictive as they were developed via data splitting (70% training and 15% for validation and 15% for testing), this was not the case for the RSM model. Moreover, the FC-CCD study data used in this case was directly related to the developed RSM models. Thus, to further provide deeper insight into the predictive performance of these two models, their potential for predicting

equilibrium and kinetic behaviors from different experiments were studied and results are presented in the sections below.

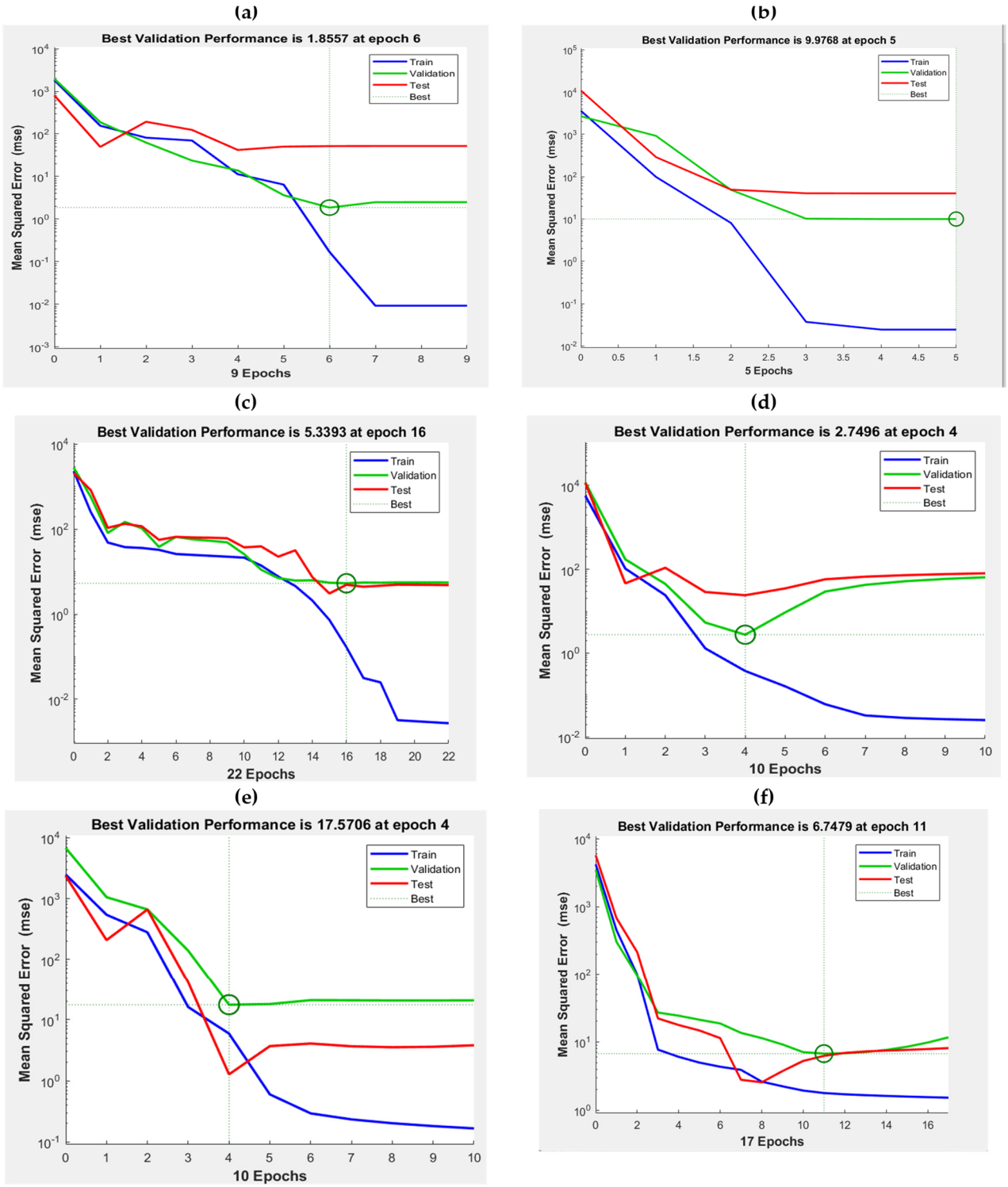

Figure 9. ANN-LMA model optimization strategy for FC-CCD (**a**,**b**); thermodynamics (**c**,**d**) and kinetics for Qe1 and Qe2 (**e**,**f**).

Table 6. ANN-LMA and RSM fitted model parameters for FC-CCD, equilibrium and kinetic studies.

	Model	Parameter	Qe1	Qe2
FC-CCD study	RSM	R^2	0.999	0.997
		RMSE	0.195	1.774
	ANN-LMA	No. of neurons	5	10
		Epoch	6	5
		Training R^2	0.999	0.999
		Validation R^2	0.998	0.999
		Testing R^2	0.903	0.999
		Overall R^2	0.995	0.997
		RMSE	3.092	2.982
Cr(VI) uptake Equilibrium study	RSM	R^2	0.8715	0.9793
		RMSE	20.50	8.00
	ANN-LMA	No. of neurons	7	10
		Epoch	10	4
		Training R^2	0.998	0.999
		Validation R^2	0.905	0.966
		Testing R^2	0.995	0.982
		Overall R^2	0.993	0.992
		RMSE	4.089	4.99
Cr(VI) uptake Kinetics study	ANN-LMA	No. of neurons	10	10
		Epoch	4	17
		Training R^2	0.996	0.999
		Validation R^2	0.999	0.998
		Testing R^2	0.995	0.995
		Overall R^2	0.999	0.998
		RMSE	17.32	6.75

3.5.2. ANN and RSM Prediction of Equilibrium and Thermodynamics of Cr(VI) Uptake

Adsorption equilibrium and thermodynamics studies are traditionally indispensable for elucidating the mechanisms for removal of pollutants from water and wastewater [42]. This owes to the fact that they help to explain the rate of distribution and interactions between adsorbent surface and adsorbate in aqueous phase as described by various isotherm models (such as Langmuir, Freundlich and Elovic) which are vital for the design of reactor volumes for an effective adsorptive remediation process. Thus, excellent prediction of equilibrium and thermodynamic behaviors of adsorbate via modeling technique is of paramount importance in adsorption studies. Table 7 provides a recent review on the utilization of various LDH-based adsorbents for aqueous phase Cr(VI) uptake reported by a number of researchers [20–24]. Evidently, from this review, the most widely fitted equilibrium models that predominantly describe Cr(VI) aqueous uptake are Langmuir and Freundlich models. Similarly, as per the best fittings of the experimental data in this study and earlier related work [18], these two (2) models were adopted for understanding the predictive performances of the developed ANN-LMA and RSM models for kinetic and thermodynamic parameters for Cr(VI) adsorption onto the CoAl-LDH and bentonite-CoAl-LDH.

The ANN-LMA and RSM models' prediction abilities for the equilibrium and thermodynamic parameters were based on a separate equilibrium study (different from FC-CCD study as provided in Supplementary Material, Table S21). Their respective performances are presented in Table 6 and Figure 11a,b for Qe1 and Qe2, respectively.

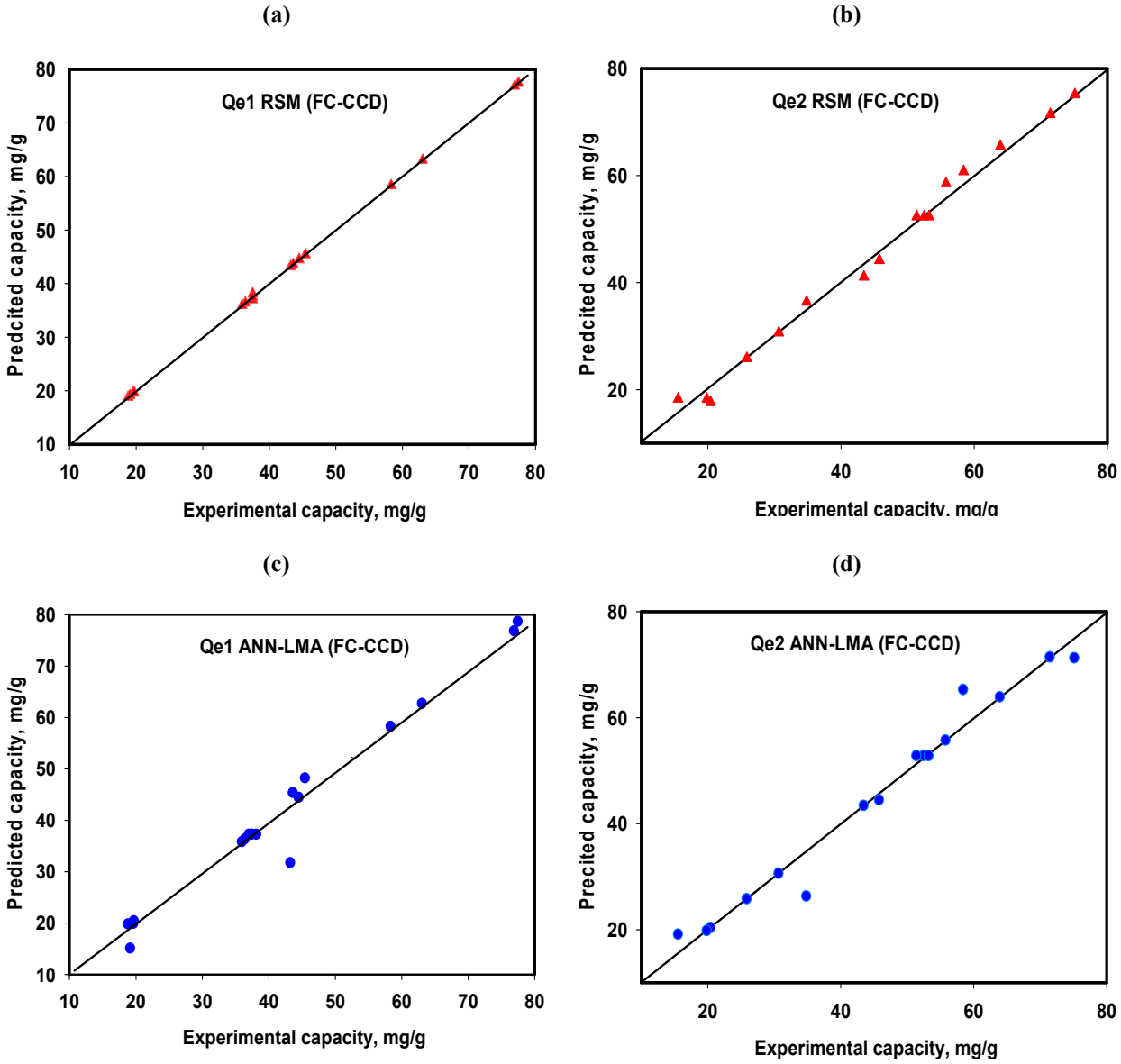

Figure 10. Predicted vs Experimental vs. plots for Qe1 and Qe2 for RSM FCC-CD (**a**,**b**) and ANN-LMA models (**c**,**d**).

It is obvious from the results that the fittings for the RSM models of the equilibrium data were lower compared with the FC-CCD data prediction as the R^2 declined to 0.872 and 0.979 (from 0.999 and 0.998) while the RMSE depreciated to 20.5 and 8.0 (from 0.195 and 1.774), respectively. Meanwhile, the ANN-LMA model R^2 of 0.993 and 0.992 (from 0.995 and 0.997) for the equilibrium data set indicate a consistent and insignificant decline in its prediction's potentials when compared with the FC-CCD data predictions. This is further confirmed by considering the corresponding RMSE of 4.089 and 4.99 (from 3.092 and 2.982). This is clearly manifested in Y = X line (Figure 11) depicting the two models' prediction potentials which indicates better performances for the ANN-LMA. Figure 11a and 11b for the RSM show much wider dispersions of the experimental vs. predicted data compared to ANN-LMA in Figure 11c,d for Qe1 and Qe2. The ANN-LMA model parameters further validate the outstanding performance of the ANN-LMA models in predicting Cr(VI) equilibrium Qe1 and Qe2 data, in spite of the FC-CCD data set approach limitations of fewer test data which could have undermined the predictive ability of ANN-LMA performance as the case was with the RSM model.

Table 7. Comparison of CoAl-LDH and its bentonite-CoAl-LDH uptake capacities with other LDH-based adsorbents for Cr(VI) uptake.

#	LDH	q_{max} (mg/g)	Model's Fittings		Reference
			Isotherm	Kinetics	
1	CoAl-LDH	121.1	Langmuir	Pseudo-second-order	This study
2	Bentonite-CoAl-LDH	205.2	Langmuir	Pseudo-second-order	This study
3	CuFeCr-LDH	22.24	Langmuir	Pseudo-second-order	[20]
4	F-U-MgAl-LDH	7.26	Freundlich	Pseudo-second-order	[43]
5	Co_2Fe_1-CO_3-LDH	5.44	Langmuir and Freundlich	Pseudo-second-order	[21]
	FeS modified FeAl-LDH	147.7	Langmuir		[32]
7	Co-Al-LDH@Fe_2O_3/3DPCNF	400.40	Sips		[33]
8	MnFe-LDH/$MnFe_2O_3$@3DNF	564.88	Langmuir, Freundlich and Sips	Pseudo-second-order	[44]
9	Fe_3O_4@SiO_2@MgAl-borate LDH	86.73	Langmuir	Pseudo-second-order	[22]
10	ZnNiCr-LDH	28.2	Langmuir	Pseudo-second-order	[23]
11	PANI@ZNd-ZnAl-LDH	219	Langmuir	Pseudo-second-order	[45]
12	Mo_3S_{13}-MgAl-LDH	90.6			[46]
13	Al-Li/Th-LDH@CNT	172.4			[24]
14	Zn-Al-Fe-LDH	52.63	Langmuir	Pseudo-second-order	[47]

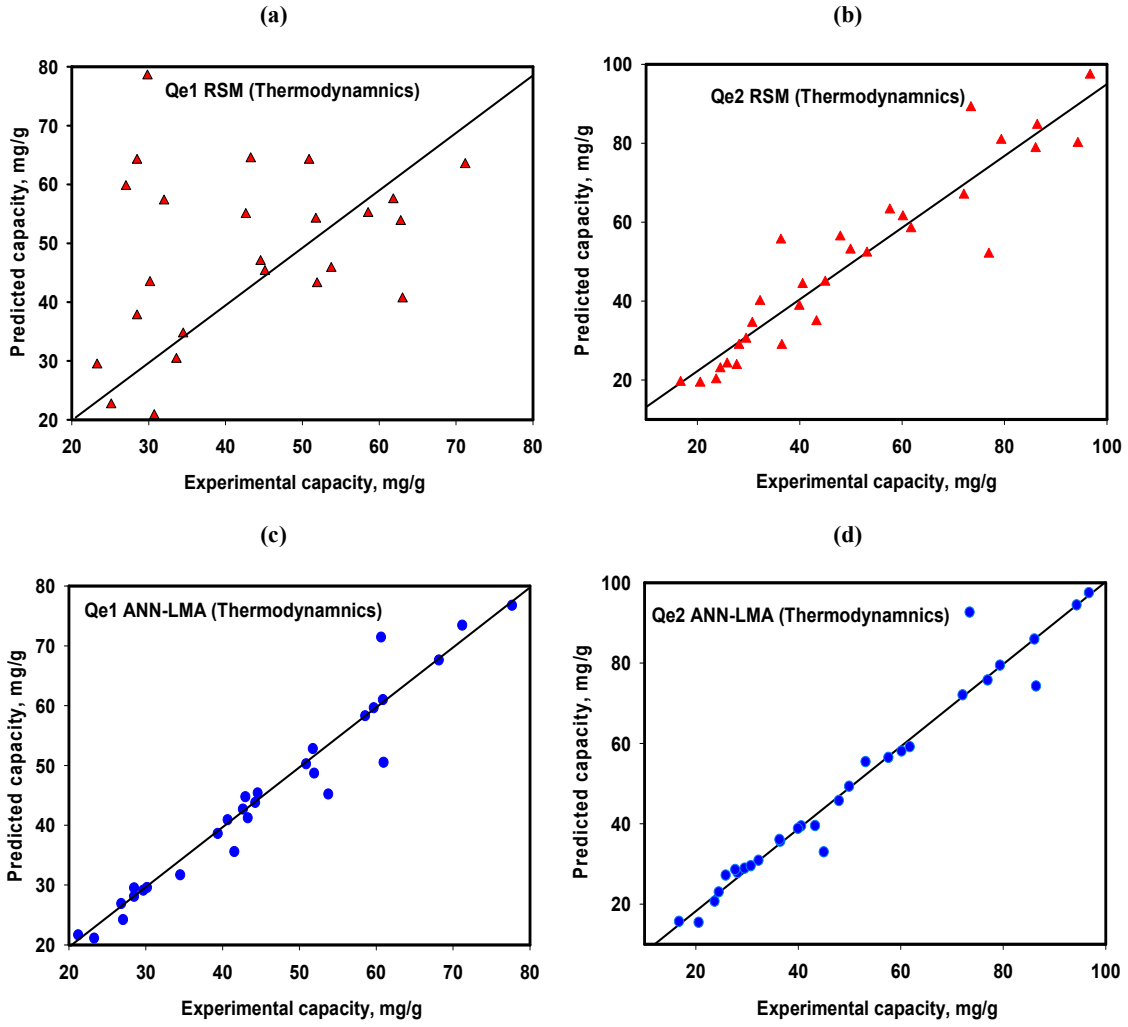

Figure 11. Experimental vs. predicted plots RSM FCC-CD (**a**,**b**) and ANN-LMA models (**c**,**d**) for thermodynamics of Cr(VI) uptake by CoAl-LDH and bentonite-CoAl-LDH.

Meanwhile, for the equilibrium study operating at different temperatures of 25, 35 and 45 °C, the predictive performances of ANN-LMA and RSM models for Cr(VI) uptake equilibrium and thermodynamic model parameters were studied. Moreover, under each model scenario (RSM and ANN-LMA), parameter predictions were carried out by employing the non-linearized and linearized forms of the investigated equilibrium and thermodynamic models, and the results are compared with the actual data (from experiment) based on R^2 and RMSE. The estimated Freundlich and Langmuir models parameters (q_{max}, K_L K_F and $1/n$) presented in Table 8 for the non-linear forms of the models also reveal better performances for the ANN-LMA models' prediction compared with the RSM models. On the other hand, employing the linearized models resulted in lower predictability of both ANN-LMA and RSM models (Table S3).

Table 8. Non-linear equilibrium model fitting parameters CoAl-LDH and bentonite-CoAl-LDH for Cr(VI) uptake.

				CoAl-LDH			Bentonite-CoAl-LDH		
Model	**Mathematical Representation**	**Temp**	**Parameter**	**Exp**	**ANN**	**RSM**	**Exp**	**ANN**	**RSM**
Langmuir	$qe = \frac{q_{max} K_L C_e}{1+K_L C_e}$	25 °C	R^2	0.9540	0.9915	0.9937	0.9665	0.9608	0.9937
			RMSE	6.9909	2.1665	2.9127	7.6944	8.5455	2.9127
			q_{max}, mg/g	121.1374	107.1379	173.0420	197.1809	199.2454	173.0420
			K_L, L/mg	0.0215	0.0228	0.0127	0.0104	0.0099	0.0127
Freundlich	$q_e = K_F {C_e}^{1/n}$		R^2	0.9164	0.9940	0.9770	0.9498	0.9407	0.9770
			RMSE	9.2974	2.4131	5.3478	9.4950	10.4106	5.3478
			K_F	9.1121	8.9650	5.9300	4.9316	4.7647	5.9300
			1/n	0.4777	0.4611	0.6073	0.6558	0.6601	0.6073
Langmuir	$qe = \frac{q_{max} K_L C_e}{1+K_L C_e}$	35 °C	R^2	0.9975	0.9879	0.9988	0.9556	0.9785	0.9882
			RMSE	1.3884	1.7969	0.5705	8.5942	3.6328	2.7187
			q_{max}, mg/g	99.2234	103.1155	91.4632	168.8715	183.0309	172.9810
			K_L, L/mg	0.0117	0.0107	0.0137	0.0074	0.0067	0.0082
Freundlich	$q_e = K_F {C_e}^{1/n}$		R^2	0.9945	0.9914	0.9978	0.9464	0.9781	0.9981
			RMSE	1.3988	1.8627	1.0008	8.2754	4.3301	1.1371
			K_F	3.2380	3.0059	3.7754	2.7190	2.6078	3.3154
			1/n	0.6093	0.6247	0.5737	0.7118	0.7243	0.6860
Langmuir	$qe = \frac{q_{max} K_L C_e}{1+K_L C_e}$	45 °C	R^2	0.9732	0.9864	0.5030	0.8683	0.9366	0.9110
			RMSE	3.3437	1.6923	22.3500	9.4967	6.3515	4.7371
			q_{max}, mg/g	149.7940	123.1122	157.0474	205.1537	172.3274	229.0193
			K_L, L/mg	0.0058	0.0071	0.0074	0.0039	0.0056	0.0028
Freundlich	$qe = K_F {C_e}^{1/n}$		R^2	0.9773	0.9913	0.4356	0.8870	0.9519	0.9329
			RMSE	3.5550	1.6221	24.1229	9.6128	6.1043	4.7517
			K_F	1.7519	1.9420	2.2258	1.5687	1.9947	1.1804
			1/n	0.7467	0.7089	0.7360	0.7812	0.7441	0.8084

The ANN-LMA and RSM models predicted Langmuir constants K_L in L/mg (Table 9) is converted to L/mmol as K_d, from which the thermodynamics parameters (Gibbs free $\Delta G°$, energy enthalpy ΔH and entropy change ΔS) were further estimated and compared with those obtained from the experiment data (i.e., actual values). At temperatures of 25, 35 and 45 °C, the values $\Delta G°$ were calculated using Equation (7) from which ΔS and ΔH, as listed in Table 9, were estimated using slope and intercepts from the linear plot between Ln (K_d) and 1/T in Equation (8).

$$\Delta G = -RT \ln K_d \tag{7}$$

$$\ln K_d = \frac{\Delta S}{R} - \frac{\Delta H}{RT} \tag{8}$$

Table 9. CoAl-LDH and bentonite-CoAl-LDH for Cr(VI) uptake thermodynamic parameter model fittings.

Adsorbent	Temp	ΔG (kJ/mol)			K_d (L/mmol)			Δ*H* (kJ/mol)			Δ*S* (kJ/mol K)		
		Actual	ANN	RSM	Actual	ANN	RSM	Actual	ANN	RSM	Actual	ANN	RSM
CoAl-LDH	25 °C	−17.386	−17.541	−16.082	0.0215	0.0228	0.0127						
	35 °C	−16.410	−16.196	−16.827	0.0117	0.0107	0.0137	−51.815	−46.421	−21.073	−0.115	−0.097	−0.016
	45 °C	−15.071	−15.611	−15.726	0.0058	0.0071	0.0074						
Bentonite-CoAl-LDH	25 °C	−15.584	−15.480	−16.082	0.0104	0.0099	0.0127						
	35 °C	−15.254	−14.982	−15.500	0.0074	0.0067	0.0082	−38.041	−22.988	−59.576	−0.075	−0.025	−0.145
	45 °C	−14.067	−14.982	−13.143	0.0039	0.0056	0.0028						

The results presented in Table 8 and Table S3 further establish the superiority of the ANN-LMA over the RSM predictions and the non-linearized forms of the Langmuir models in predicting the thermodynamics parameters. The parameters predicted using the non-linear models predicted $-\Delta G^{\circ}$, $-\Delta H$ and $-\Delta S$ for both ANN-LMA and RSM models which supported the feasibility, spontaneous nature and greater order of reaction during the Cr(VI) uptake onto the CoAl-LDH and bentonite-CoAl-LDH as obtained from the actual experiments. Moreover, they all supported the exothermic nature of the process confirming the RSM-FC-CCD modeling results (Section 3.2.3). However, using the linear Langmuir model K_L values resulted in obtaining some $+\Delta H$ and $+\Delta S$ conflicting with the expected negative actual values. Additionally, the linear models were also characterized with poor predictions, which was mainly observed with the RMS models.

3.5.3. ANN Prediction of Kinetic of Cr(VI) Uptake

In addition to equilibrium and thermodynamic behaviors, kinetic behaviors are usually needed to help further comprehend the mechanisms for removal of pollutants from aqueous solutions in addition to designing the reactor volume necessary for an effective adsorptive remediation process. Consequently, predictive models capable of capturing the kinetic behaviors are also vital in adsorption studies. Thus, based on the different Cr(VI) initial concentrations (20, 60 and 100 mg/L) that were studied, the kinetics of Cr(VI) onto the two LDH-based adsorbents were investigated. The ANN-LMA prediction abilities of the Cr(VI) kinetic parameters were also based on a separate study (different from FC-CCD study), and as a consequence of lack of time variable in the FC-CCD, the developed RSM-FCC-CD model cannot be employed for predicting the kinetic parameters in this study. Thus, the predictive performances of the ANN-LMA for Cr(VI) uptake onto the CO-Al-LDH and bentonite-CoAl-LDH nanocomposites are provided in Table 6 and depicted in Figure 12a,b for Qe1 and Qe2, respectively (experimental data in Supplementary Material Table S3).

The ANN-LMA model effectively captured the kinetic data and provided similar R^2 of 0.999 and 0.998 with corresponding 17.32 and 6.75 for Qe1 and Qe2 which is demonstrated by in line Y = X (Figure 12). Additionally, the ANN-LMA models' predictive performances of Cr(VI) uptake kinetic model parameters for pseudo-first and pseudo-second-order were investigated. Moreover, under each model scenario (pseudo-first or pseudo-second-order), parameter predictions were undertaken via employing the non-linearized and linearized forms of the kinetic models and the results are compared with the actual experimental data. The predicted kinetic parameters (qe, k_1 and k_2) presented in Table 10 for the non-linear forms of the models indicate excellent performances for the ANN-LMA models. Moreover, employing the non-linearized kinetic models consistently revealed better predictive capacities as in the case of the equilibrium and thermodynamics (Table S3). Interestingly, all the ANN-LMA model predictions conform with the actual experimental data, which establishes that CoAl-LDH and bentonite-CoAl-LDH Cr(VI) uptake was mainly described by pseudo-second-order kinetics compared to pseudo-first-order as presented in Table 8. This corroborates with earlier studies on Cr(VI) adsorption onto different types of LDHs that reported the predominate second order model fitting (Table 7) [20–24]. Thus, taking into account these related works and many other published classical works under this subject, chemisorption was the main mechanism that significantly controlled the Cr(VI)

uptake by both CoAl-LDH and bentonite-CoAl-LDH, which are well established by the ANN-LMA model predictions.

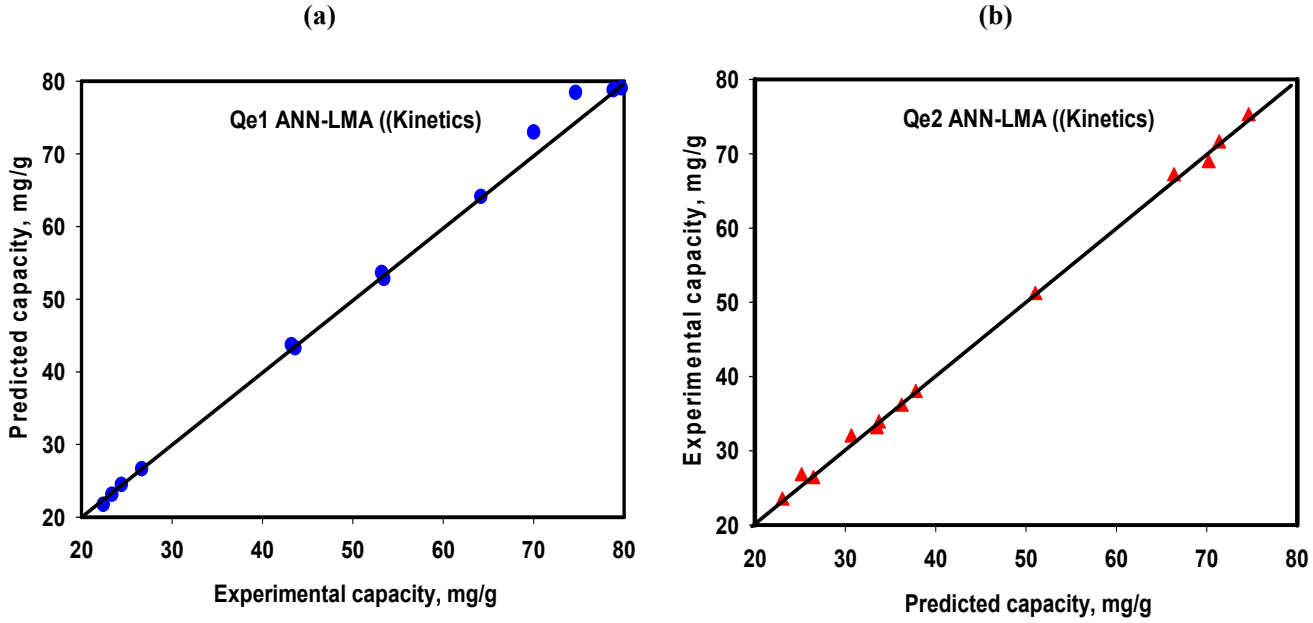

Figure 12. ANN-LMA model predictive performance for Cr(VI) uptake kinetics for CoAl-LDH (**a**) and bentonite-CoAl-LDH (**b**).

Table 10. Non-linear kinetic model fitting parameters for CoAl-LDH and bentonite-CoAl-LDH for Cr(VI) uptake.

Model	Mathematical Representation	Initial Concentration		CoAl-LDH		Bentonite-CoAl-LDH	
			Parameter	Exp	ANN-LMA	Exp	ANN-LMA
Pseudo-first-order	$q_t = q_e(1 + e^{-k_1 t})$	20	R^2	0.915	0.946	0.968	0.997
			RMSE	2.260	2.383	3.079	0.858
			q_e	19.741	20.130	34.273	20.191
			k_1	0.112	0.089	0.060	2.541
		60	R^2	0.909	0.797	0.830	0.995
			RMSE	3.020	3.714	5.404	15.266
			q_e	54.290	52.530	75.312	62.394
			k_1	0.0131	0.0143	0.0229	1.7765
		100	R^2	0.996	0.997	0.959	0.944
			RMSE	1.636	1.722	10.479	10.748
			q_e	78.458	80.353	89.023	104.268
			k_1	0.080	0.079	0.139	0.094
Pseudo-second-order	$q_t = \frac{q_e k_2{}^2\ t}{1+q_e k_2\ t}$	20	i^2	0.966	0.985	0.997	0.997
			RMSE	1.368	1.519	1.936	0.860
			qe	21.596	21.992	38.333	20.187
			k_2	0.008	0.006	0.002	149.352
		60	R^2	0.936	0.841	0.885	0.995
			RMSE	2.947	3.598	4.109	15.268
			qe	74.174	68.898	92.254	62.398
			k_2	0.0001	0.0002	0.0002	29.6852
		100	R^2	0.987	0.606	0.987	0.887
			RMSE	9.734	19.190	24.534	12.479
			qe	85.389	473.750	95.008	0.001
			k_2	0.001	64.717	0.003	110.570

The forgone results analysis shows the potential and prowess of the ANN-LMA models in yielding excellent prediction results compared to the RSM models. Thus, the superiority and credibility of the ANN-LMA is further established in this study, considering the uniqueness of its approach to data splitting, which completely contrasted the RSM technique. Moreover, despite the few numbers of experimental runs for the FC-CCD, the ANN-LMA model performances were still quite comparative to the RSM models. These further demonstrate the higher data quality credibility in ANN-LMA models.

Although, the RSM provide avenues for producing a distinct mathematical relationship between input and output variables as well as visual display of these relationships, yet it requires a specific experimental design such as FC-CCD adopted in this study. In contrast, ANN does not need prior experimental design to be adopted and it is neither bound nor restricted by mathematical relationship. This suggests that the ANN-LMA models are more reliable in capturing Cr(VI) adsorption data for the CoAl-LDH and bentonite-CoAl-LDH composites, corroborating earlier studies [48–50]. However, it is important to note that both the RSM and ANN-LMA models presented pose inherent limitations considering that further influence of independent variable analysis and sensitivity analysis on their equilibrium, kinetic and thermodynamic predictability are needed to further establish their potentials [12].

4. Conclusions

In this study, the adsorptive performances of CoAl-LDH and its intercalated bentonite-CoAl (bentonite-CoAl-LDH) for removal of Cr(VI) from water were modeled using artificial neural network (ANN)-based algorithms and response surface methodology (RSM) and compared based on coefficient of determination (R^2) and root mean square error (RMSE). Based on the results obtained, the following conclusions were reached:

1. The Cr(VI) uptake capacity data obtained for the adsorbents effectively fits the quartic RSM polynomial models (R^2 = 0.997) with insignificant lack of fit (p-value < 0.05).
2. The Cr (VI) uptake capacity improved with increasing Cr(VI) initial concentration and initial pH, while increasing the operational temperature with optimal conditions obtained at temperature 25 °C, pH = 2 and 126 mg/L initial Cr(VI) concentration.
3. Levenberg-Marquardt ANN algorithms (ANN-LMA) converged faster and better compared to other tested ANN-based algorithms.
4. Both the RSM and ANN-LMA models performed well and based on the non-linear Langmuir model K_L values, they predicted $-\Delta G^{\circ}$, $-\Delta H$ and $-\Delta S$ which supported the actual feasibility, spontaneity and greater order of reaction as well as the exothermic nature of Cr(VI) uptake onto the tested adsorbents.
5. The ANN-LMA models' accurate kinetic parameter predictions further indicated a mainly pseudo-second-order process conforming the predominant chemisorption mechanism, which are well established by the Cr(VI) speciation and surface charges for the Cr(VI) uptake by both CoAl-LDH and bentonite-CoAl-LDH.
6. The ANN-LMA models' predictions were better compared to the RSM predictions, and the non-linearized forms of the kinetics and equilibrium models provided better parameters compared to the linearized forms.
7. The ANN-LMA models indicated a consistent and insignificant decline in their prediction potentials under the different mechanistic studies undertaken.
8. This study demonstrates the high potential reliability of RSM and ANN-LMA models in capturing Cr(VI) adsorption data for LDHs nanocomposites heavy metal uptake in water and wastewater treatment.
9. It is recommended to undertake further studies on the influence of independent variable analysis and sensitivity analysis for the RSM and ANN-LMA models on equilibrium, kinetic, and thermodynamic predictability to further establish their potentials.

Supplementary Materials: The following supporting information can be downloaded at: https://www.mdpi.com/article/10.3390/w14101644/s1. Table S1: Developed bentonite-CoAl-LDH Cr(VI) uptake capacity (Qe1) model numerical optimization target objectives and results; Table S2: Thermodynamics Experimental study experimental variables and results; Table S3: Kinetics study experimental variables and results; Table S4: Linear equilibrium models fittings parameters CoAl-LDH and bentonite-CoAl-LDH for Cr(VI) uptake; Table S5: CoAl-LDH and Bentonite-CoAl-LDH for Cr(VI) uptake thermodynamic parameters.

Funding: The author acknowledges the support provided by Deanship of Scientific Research through funding Project 2020-112-Eng at NSTIP at Imam Abdulrahman Bin Faisal University, Dammam KSA.

Data Availability Statement: Not applicable.

Acknowledgments: The author acknowledges the support provided by Imam Abdulrahman Bin Faisal University for the facilities provided for conducting this research.

Conflicts of Interest: The author declares no conflict of interest.

References

1. Reynel-Ávila, H.E.; Aguayo-Villarreal, I.A.; Diaz-Muñoz, L.L.; Moreno-Pérez, J.; Sánchez-Ruiz, F.J.; Rojas-Mayorga, C.K.; Mendoza-Castillo, D.I.; Bonilla-Petriciolet, A. A Review of the Modeling of Adsorption of Organic and Inorganic Pollutants from Water Using Artificial Neural Networks. *Adsorpt. Sci. Technol.* **2022**, *2022*, 9384871. [CrossRef]
2. Haladu, S.A.; Dalhat Mu'azu, N.; Ali, S.A.; Elsharif, A.M.; Odewunmi, N.A.; Abd El-Lateef, H.M. Inhibition of mild steel corrosion in 1 M H2SO4 by a gemini surfactant 1,6-hexyldiyl-bis-(dimethyldodecylammonium bromide): ANN, RSM predictive modeling, quantum chemical and MD simulation studies. *J. Mol. Liq.* **2022**, *350*, 118533. [CrossRef]
3. Yaseen, Z.M. An insight into machine learning models era in simulating soil, water bodies and adsorption heavy metals: Review, challenges and solutions. *Chemosphere* **2021**, *277*, 130126. [CrossRef] [PubMed]
4. Olatunji, O.O.; Akinlabi, S.; Madushele, N.; Adedeji, P.A. Property-based biomass feedstock grading using k-Nearest Neighbour technique. *Energy* **2020**, *190*, 116346. [CrossRef]
5. Syah, R.; Piri, F.; Elveny, M.; Khan, A. Artificial Intelligence simulation of water treatment using nanostructure composite ordered materials. *J. Mol. Liq.* **2021**, *345*, 117046. [CrossRef]
6. Myers, R.H.; Montgomery, D.C.; Anderson-Cook, C.M. *Response Surface Methodology: Process and Product Optimization Using Designed Experiments*; John Wiley & Sons: New York, NY, USA, 2016; ISBN 1118916034.
7. Karaman, C.; Karaman, O.; Show, P.-L.; Karimi-Maleh, H.; Zare, N. Congo red dye removal from aqueous environment by cationic surfactant modified-biomass derived carbon: Equilibrium, kinetic, and thermodynamic modeling, and forecasting via artificial neural network approach. *Chemosphere* **2022**, *290*, 133346. [CrossRef]
8. Gadekar, M.R.; Ahammed, M.M. Modelling dye removal by adsorption onto water treatment residuals using combined response surface methodology-artificial neural network approach. *J. Environ. Manag.* **2019**, *231*, 241–248. [CrossRef]
9. Mu'azu, N.D.; Jarrah, N.; Zubair, M. A comparison of ann and rsm models for anionic dye adsorption onto bentonite-clay intercalated cobalt-aluminum ldh nanocomposites. *Desalin. Water Treat.* **2020**, *179*, 340–353. [CrossRef]
10. Fetimi, A.; Dâas, A.; Benguerba, Y.; Merouani, S.; Hamachi, M.; Kebiche-Senhadji, O.; Hamdaoui, O. Optimization and prediction of safranin-O cationic dye removal from aqueous solution by emulsion liquid membrane (ELM) using artificial neural network-particle swarm optimization (ANN-PSO) hybrid model and response surface methodology (RSM). *J. Environ. Chem. Eng.* **2021**, *9*, 105837. [CrossRef]
11. Alara, O.R.; Abdurahman, N.H.; Afolabi, H.K.; Olalere, O.A. Efficient extraction of antioxidants from Vernonia cinerea leaves: Comparing response surface methodology and artificial neural network. *Beni-Suef Univ. J. Basic Appl. Sci.* **2018**, *7*, 276–285. [CrossRef]
12. Dalhat, M.A.; Mu'Azu, N.D.; Essa, M.H. Generalized decay and artificial neural network models for fixed-Bed phenolic compounds adsorption onto activated date palm biochar. *J. Environ. Chem. Eng.* **2021**, *9*, 104711. [CrossRef]
13. Zamora-Ledezma, C.; Negrete-Bolagay, D.; Figueroa, F.; Zamora-Ledezma, E.; Ni, M.; Alexis, F.; Guerrero, V.H. Heavy metal water pollution: A fresh look about hazards, novel and conventional remediation methods. *Environ. Technol. Innov.* **2021**, *22*, 101504. [CrossRef]
14. Kapoor, D.; Singh, M.P. Heavy metal contamination in water and its possible sources. In *Heavy Metals in the Environment*; Elsevier: Amsterdam, The Netherlands, 2021; pp. 179–189.
15. Chaillot, D.; Bennici, S.; Brendlé, J. Layered double hydroxides and LDH-derived materials in chosen environmental applications: A review. *Environ. Sci. Pollut. Res.* **2021**, *28*, 24375–24405. [CrossRef] [PubMed]
16. Yu, G.; Wang, X.; Liu, J.; Jiang, P.; You, S.; Ding, N.; Guo, Q.; Lin, F. Applications of nanomaterials for heavy metal removal from water and soil: A review. *Sustainability* **2021**, *13*, 713. [CrossRef]
17. Qiu, B.; Tao, X.; Wang, H.; Li, W.; Ding, X.; Chu, H. Biochar as a low-cost adsorbent for aqueous heavy metal removal: A review. *J. Anal. Appl. Pyrolysis* **2021**, *155*, 105081. [CrossRef]

18. Jarrah, N.; Mu'azu, N.D.; Zubair, M.; Al-Harthi, M. Enhanced adsorptive performance of Cr(VI) onto layered double hydroxide-bentonite composite: Isotherm, kinetic and thermodynamic studies. *Sep. Sci. Technol.* **2020**, *55*, 1897–1909. [CrossRef]
19. Zubair, M.; Daud, M.; McKay, G.; Shehzad, F.; Al-Harthi, M.A. Recent progress in layered double hydroxides (LDH)-containing hybrids as adsorbents for water remediation. *Appl. Clay Sci* **2017**, *143*, 279–292. [CrossRef]
20. Zhang, Y.; Jing, C.; Zheng, J.; Yu, H.; Chen, Q.; Guo, L.; Pan, D.; Naik, N.; Shao, Q.; Guo, Z. Microwave hydrothermal fabrication of CuFeCr ternary layered double hydroxides with excellent Cr(VI) adsorption. *Colloids Surf. A Physicochem. Eng. Asp.* **2021**, *628*, 127279. [CrossRef]
21. Liu, W.; Yu, Y. Ultrafast advanced treatment of chromium complex-containing wastewater using Co/Fe layered double hydroxide. *Environ. Technol. Innov.* **2022**, *26*, 102296. [CrossRef]
22. Miao, J.; Zhao, X.; Zhang, Y.-X.; Liu, Z.-H. Feasible synthesis of hierarchical porous MgAl-borate LDHs functionalized Fe_3O_4@SiO_2 magnetic microspheres with excellent adsorption performance toward congo red and Cr(VI) pollutants. *J. Alloys Compd.* **2021**, *861*, 157974. [CrossRef]
23. Guo, L.; Zhang, Y.; Zheng, J.; Shang, L.; Shi, Y.; Wu, Q.; Liu, X.; Wang, Y.; Shi, L.; Shao, Q. Synthesis and characterization of ZnNiCr-layered double hydroxides with high adsorption activities for Cr(VI). *Adv. Compos. Hybrid Mater.* **2021**, *4*, 819–829. [CrossRef]
24. Manea, Y.K.; Khan, A.M.; Wani, A.A.; Saleh, M.A.S.; Qashqoosh, M.T.A.; Shahadat, M.; Rezakazemi, M. In-grown flower like Al-Li/Th-LDH@CNT nanocomposite for enhanced photocatalytic degradation of MG dye and selective adsorption of Cr (VI). *J. Environ. Chem. Eng.* **2022**, *10*, 106848. [CrossRef]
25. Mu'azu, N.D.; Jarrah, N.; Kazeem, T.S.; Zubair, M.; Al-Harthi, M. Bentonite-layered double hydroxide composite for enhanced aqueous adsorption of Eriochrome Black T. *Appl. Clay Sci.* **2018**, *161*, 23–34. [CrossRef]
26. Zhu, X.; Wang, X.; Liu, K.; Zhou, S.; Alqsair, U.F.; El-Shafay, A.S. Machine learning simulation of Cr (VI) separation from aqueous solutions via a hierarchical nanostructure material. *J. Mol. Liq.* **2022**, *350*, 118565. [CrossRef]
27. Ait-Amir, B.; Pougnet, P.; El Hami, A. Meta-Model Development. In *Embedded Mechatronic Systems 2*; El Hami, A., Pougnet, P.B.T.-E.M.S., Eds.; Elsevier: Amsterdam, The Netherlands, 2020; pp. 157–187, ISBN 978-1-78548-190-1.
28. Elkhider, K.H.A.; Ihsanullah, I.; Zubair, M.; Manzar, M.S.; Mu'azu, N.D.; Al-Harthi, M.A. Synthesis, Characterization and Dye Adsorption Performance of Strontium Ferrite decorated Bentonite-CoNiAl Magnetic Composite. *Arab. J. Sci. Eng.* **2020**, *45*, 7397–7408. [CrossRef]
29. Blaisi, N.I.; Zubair, M. Date palm ash-MgAl-layered double hydroxide composite: Sustainable adsorbent for effective removal of methyl orange and eriochrome black-T from aqueous phase. *Environ. Sci. Pollut. Res.* **2018**, *25*, 34319–34331. [CrossRef]
30. Waheed, A.; Kazi, I.W.; Manzar, M.S.; Ahmad, T.; Mansha, M.; Ullah, N.; Ahmed Blaisi, N.I. Ultrahigh and efficient removal of Methyl orange, Eriochrom Black T and acid Blue 92 by triazine based cross-linked polyamine resin: Synthesis, isotherm and kinetic studies. *Colloids Surf. A Physicochem. Eng. Asp.* **2020**, *607*, 125472. [CrossRef]
31. Shan, R.; Yan, L.; Yang, Y.; Yang, K.; Yu, S.; Yu, H.; Zhu, B.; Du, B. Highly efficient removal of three red dyes by adsorption onto Mg–Al-layered double hydroxide. *J. Ind. Eng. Chem.* **2015**, *21*, 561–568. [CrossRef]
32. Zhang, S.; Zhang, W.; Wan, Y. Adsorption and Reduction of Aqueous Cr by FeS-Modified Fe-Al Layered Double Hydroxide. *Sustainability* **2021**, *14*, 21. [CrossRef]
33. Poudel, M.B.; Awasthi, G.P.; Kim, H.J. Novel insight into the adsorption of Cr(VI) and Pb(II) ions by MOF derived Co-Al layered double hydroxide @hematite nanorods on 3D porous carbon nanofiber network. *Chem. Eng. J.* **2021**, *417*, 129312. [CrossRef]
34. Sheng, G.; Hu, J.; Li, H.; Li, J.; Huang, Y. Enhanced sequestration of Cr(VI) by nanoscale zero-valent iron supported on layered double hydroxide by batch and XAFS study. *Chemosphere* **2016**, *148*, 227–232. [CrossRef] [PubMed]
35. Yuan, X.; Wang, Y.; Wang, J.; Zhou, C.; Tang, Q.; Rao, X. Calcined graphene/MgAl-layered double hydroxides for enhanced Cr(VI) removal. *Chem. Eng. J.* **2013**, *221*, 204–213. [CrossRef]
36. Zhao, J.; Zhang, X.; He, X.; Xiao, M.; Zhang, W.; Lu, C. A super biosorbent from dendrimer poly (amidoamine)-grafted cellulose nanofibril aerogels for effective removal of Cr (VI). *J. Mater. Chem. A* **2015**, *3*, 14703–14711. [CrossRef]
37. Naja, G.; Volesky, B. The Mechanism of Metal Cation and Anion Biosorption. In *Microbial Biosorption of Metals*; Kotrba, P., Mackova, M., Macek, T., Eds.; Springer: Dordrecht, The Netherlands, 2011; pp. 19–58, ISBN 978-94-007-0443-5.
38. Yadav, A.M.; Nikkam, S.; Gajbhiye, P.; Tyeb, M.H. Modeling and optimization of coal oil agglomeration using response surface methodology and artificial neural network approaches. *Int. J. Miner. Process.* **2017**, *163*, 55–63. [CrossRef]
39. Khamparia, A.; Pandey, B.; Pandey, D.K.; Gupta, D.; Khanna, A.; de Albuquerque, V.H.C. Comparison of RSM, ANN and Fuzzy Logic for extraction of Oleonolic Acid from Ocimum sanctum. *Comput. Ind.* **2020**, *117*, 103200. [CrossRef]
40. Ray, S.; Haque, M.; Ahmed, T.; Nahin, T.T. Comparison of artificial neural network (ANN) and response surface methodology (RSM) in predicting the compressive and splitting tensile strength of concrete prepared with glass waste and tin (Sn) can fiber. *J. King Saud Univ.-Eng. Sci.* **2021**. [CrossRef]
41. Nuapia, Y.; Cukrowska, E.; Tutu, H.; Chimuka, L. Statistical comparison of two modeling methods on pressurized hot water extraction of vitamin C and phenolic compounds from Moringa oleifera leaves. *S. Afr. J. Bot.* **2018**, *129*, 9–16. [CrossRef]
42. Mu'azu, N.D.; Jarrah, N.; Zubair, M.; Manzar, M.S.; Kazeem, T.S.; Qureshi, A.; Haladu, S.A.; Blaisi, N.I.; Essa, M.H.; Al-Harthi, M.A. Mechanistic aspects of magnetic MgAlNi barium-ferrite nanocomposites enhanced adsorptive removal of an anionic dye from aqueous phase. *J. Saudi Chem. Soc.* **2020**, *24*, 715–732. [CrossRef]

43. Zhang, L.; Zhao, J.; Zhang, S.; Yu, Q.; Cheng, J.; Qiu, X. Ultrasound-assisted synthesis of single layer MgAl hydrotalcite for the removal of Cr(VI) in solution and soil. *Appl. Clay Sci.* **2021**, *204*, 106025. [CrossRef]
44. Babu Poudel, M.; Shin, M.; Joo Kim, H. Interface engineering of MIL-88 derived MnFe-LDH and $MnFe_2O_3$ on three-dimensional carbon nanofibers for the efficient adsorption of Cr(VI), Pb(II), and As(III) ions. *Sep. Purif. Technol.* **2022**, *287*, 120463. [CrossRef]
45. Wani, A.A.; Khan, A.M.; Manea, Y.K.; Salem, M.A.S.; Shahadat, M. Selective adsorption and ultrafast fluorescent detection of Cr(VI) in wastewater using neodymium doped polyaniline supported layered double hydroxide nanocomposite. *J. Hazard. Mater.* **2021**, *416*, 125754. [CrossRef] [PubMed]
46. Zhang, L.; Wang, H.; Zhang, Q.; Wang, W.; Yang, C.; Du, T.; Yue, T.; Zhu, M.; Wang, J. Demand-oriented construction of Mo3S13-LDH: A versatile scavenger for highly selective and efficient removal of toxic Ag(I), Hg(II), As(III), and Cr(VI) from water. *Sci. Total Environ.* **2022**, *820*, 153334. [CrossRef] [PubMed]
47. Rezak, N.; Bahmani, A.; Bettahar, N. Adsorptive removal of P(V) and Cr(VI) by calcined Zn-Al-Fe ternary LDHs. *Water Sci. Technol.* **2021**, *83*, 2504–2517. [CrossRef] [PubMed]
48. Zhao, L.; Dai, T.; Qiao, Z.; Sun, P.; Hao, J.; Yang, Y. Application of artificial intelligence to wastewater treatment: A bibliometric analysis and systematic review of technology, economy, management, and wastewater reuse. *Process Saf. Environ. Prot.* **2020**, *133*, 169–182. [CrossRef]
49. Ghaedi, A.M.; Vafaei, A. Applications of artificial neural networks for adsorption removal of dyes from aqueous solution: A review. *Adv. Colloid Interface Sci.* **2017**, *245*, 20–39. [CrossRef]
50. Nag, S.; Bar, N.; Das, S.K. Sustainable bioremadiation of Cd(II) in fixed bed column using green adsorbents: Application of Kinetic models and GA-ANN technique. *Environ. Technol. Innov.* **2019**, *13*, 130–145. [CrossRef]